1 Introduction

Advances in technology have allowed wireless data communications technology to be implemented into everyday devices such as mobile telephones, laptop computers and personal data assistants (PDAs). This technology has been embraced by society and new applications for the technology are frequently appearing. However, a major limitation of the existing wireless technology is that the devices must be in direct transmission range of a central controller or base-station.

To overcome this limitation, a new class of device is emerging that has the ability to communicate with one another to pass messages to the base-station. This allows the devices to be used over a larger area using low power transmitters. This technology is known as an ad-hoc network and is made up of devices called nodes.

In an ad-hoc network, the nodes determine a path to the base-station by relaying messages through one another. The ad-hoc network is self-maintaining, which means that if a communication link fails, the nodes will determine a new route to the base-station through the network. Ad-hoc networks are also self-configuring, therefore, if a new node is added, the network will automatically adjust with no user intervention.

Further advances in technology have allowed ad-hoc network algorithms to be implemented on low-cost microprocessors. When these are combined with a sensing device and a small radio transceiver a wireless sensor network (WSN) can be formed. The field of wireless sensor networks is rapidly expanding, as it has a wide range of applications. These applications include environmental monitoring, battlefield monitoring, animal tracking and building structure monitoring.

The current focus of research in this field is the development of miniature power-efficient nodes. It is envisaged by companies such as Dust Networks [1] that nodes will eventually be cubic millimetres in size with several years of battery life. These tiny nodes are commonly called 'Smart Dust' and it is envisioned that millions of these devices will be produced for a plethora of applications.

A disadvantage of this research focus is that the nodes typically have a transmission range of several hundred metres. This limits the applications of this technology to small geographic areas that are covered by densely deployed nodes. This is of particular disadvantage to countries such as Australia because it does not allow the technology to be used for useful applications such as monitoring the level of water troughs on a large farm or the soil moisture content to ensure that irrigation is conducted efficiently. A long-range wireless sensor network could also be used to monitor the water condition on the Great Barrier Reef.

An aim of this thesis was to allow wireless sensor network technology to be used over large geographical areas. The main objective of this thesis was to *investigate what changes are required to existing wireless sensor nodes to allow long-range communications.*

The investigation was conducted by answering the following research questions:

- How can the long-range radio links be accurately modelled?
- What changes are needed to the node hardware?
- What changes are needed to the lower layers of the protocol stack?

The first phase of this project involved the development of a novel radio propagation model to examine the feasibility of a long-range wireless sensor network. The findings were used to create the specifications for the radio transceiver hardware, which was later integrated with a commonly-used node called the Mica2. A carrier-sense, multiple access with collision avoidance (CSMA/CA) medium access protocol and a routing protocol called MintRoute were implemented on the new long-range wireless sensor node called the JCUMote. A four-node prototype network was

deployed and tested in Townsville, Australia and the results of tests were used to refine and validate the initial radio propagation model.

This thesis describes the basic principles of wireless communication, gives an introduction to wireless sensor networks and discusses current research in this field. After this, the fundamentals of radio propagation are discussed and a novel radio propagation model is proposed for long-range wireless sensor networks. This leads to a discussion of radio transceiver design, antenna design and the development of a new long-range wireless sensor node. The results of several field-tests are presented and used to validate the radio propagation model and make recommendations on the design and deployment of a long-range wireless sensor network.

Chapter 2 introduces the network stack model which is used to represent a wireless sensor network. The fundamentals of each layer of the network stack are presented, with particular attention given to the lower layers which are the primary focus of this thesis. This chapter also identifies existing applications of wireless sensor networks and reviews the existing wireless sensor nodes.

Chapter 3 discusses the basic principles of radio propagation and proposes a novel radio propagation model for long-range wireless sensor networks. Several radio propagation predictions are shown and the chapter is concluded with a discussion of the refinements made to the model due to the results of the field testing.

Chapter 4 introduces the JCUMote, a long-range wireless sensor node. This chapter begins with a discussion of the design of the radio transceiver hardware, which includes a power amplifier, receiver isolation network and a transceiver IC. The design of a suitable antenna is also presented.

Chapter 5 presents wireless sensor network operating systems and examines TinyOS, which is implemented on the JCUMote. A discussion of the implemented network protocols is included, as well as the structure of the software applications used for field-testing.

Chapter 6 presents the results of the field tests. This includes transmitter range tests in suburban and rural environments and the field-testing of the long-range wireless sensor network. The results are compared with the radio propagation model and a novel method is presented which allows the number of multipath components to be estimated in the suburban environment. The chapter is concluded with predictions of further possible increases in the transmitter range.

The conclusions to the thesis are presented in Chapter 7, which includes a discussion of future work in the area of long-range wireless sensor networks.

2 Literature Review

This thesis investigates the possible changes required to existing wireless sensor nodes in order to achieve long-range communications. A literature review was conducted to determine the current state of the technology. This chapter contains a review of the components of existing wireless sensor networks. The literature review commences with a presentation of the network stack model which is commonly used to represent network technology. This is followed by a review of existing wireless communications technology and an overview of existing wireless sensor nodes. The chapter finishes with a discussion of the layers of the network stack when applied to wireless communications.

2.1 Overview of Network Terminology

2.1.1 The Network Protocol Stack

The operation of network devices is frequently represented using a network stack model. There are two common models: the Open System Interconnection (OSI) model and the Internet model, which are compared in Figure 2-1.

OSI	Internet
Application	Application
Presentation	
Session	TCP
Transport	
Internet	IP
Data Link	MAC
Physical	Physical

Figure 2-1: OSI Model vs. Internet Model

As seen in Figure 2-1, each network stack is made up layers that perform a specific task. Communication is between adjacent layers only. The OSI model is made up of seven layers:

- Application layer: The end-user process that requires network connectivity.
- Presentation layer: Converts data into a recognisable form for the upper layer.
- Session layer: Initialises and terminates connection between applications.
- Transport layer: Responsible for flow control and end-to-end delivery.
- Internet layer: Determines the route for packets to reach the destination node.
- Data Link layer: Assembles and disassembles packets. Controls the shared access to the communications medium and minimises message collisions.
- Physical layer: Transmits and receives data over the communications medium.

The Internet model is a simplified version of the OSI model. MAC stands for Medium Access Control and performs the same tasks as the data-link layer. IP stands for Internet Protocol and is equivalent to the OSI Internet layer. TCP stands for Transmission Control Protocol and is responsible for the same tasks as the transport and session layers. The application layer executes the same tasks as the OSI application and presentation layers.

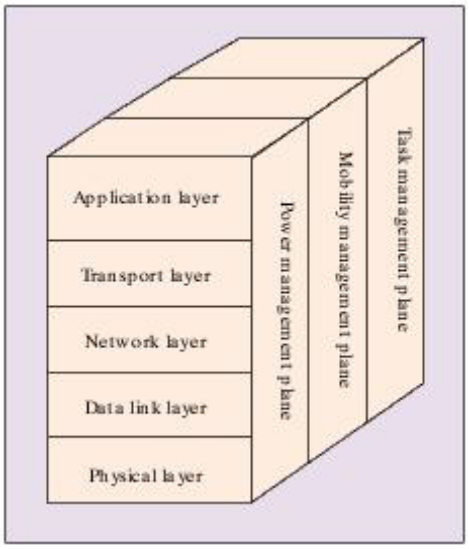

Figure 2-2: Sensor Network Protocol Stack [2]

For sensor networks, Akyildiz [2] described a sensor network protocol stack (Figure 2-2). This protocol stack is similar to the Internet stack, except that it includes three additional planes which monitor the power, movement and task management among the sensor nodes. The power management plane monitors the node's power usage and takes actions to conserve power. The mobility management plane monitors the

movement of the node and ensures that a route is available to the end node through the surrounding neighbours. The task management plane balances and schedules tasks given to a certain region. Often several nodes are positioned to monitor one parameter. Therefore, the task of monitoring may be shared amongst all nodes using a task management protocol.

2.2 The Network Stack

2.2.1 Physical Layer

The physical layer basically consists of the transceiver hardware. The field of broadcasting digital data using radio transmission techniques has been discussed extensively in the past. Akyildiz [2] stated that for a sensor network, the modulation schemes must be simple and low-power, signal propagation effects should be minimised and the hardware design should be small in size, low in power usage and low in cost.

2.2.1.1 Modulation Techniques

A review of modulation techniques is contained in Appendix A. When operating with battery powered devices it is necessary to use an output power amplifier of high efficiency, such as a class C amplifier. This PA requires a signal with a constant envelope, because non-linearities occur if the device is momentarily switched off. This means that modulation techniques such as FSK, MSK, $\pi/4$ QPSK or OQPSK must be used.

2.2.1.2 Spread-Spectrum Techniques

Spread-spectrum techniques were not employed in this thesis. However, a review of spread-spectrum techniques is included in appendix E.7 as reference material to complement the sections below.

2.2.2 Data Link Layer

The data link layer has two main roles. These are medium access control and error correction. The former process involves the establishment of communication links for data transfer. This process must be fair and efficiently share the communication resources. The error correction process is used to reduce the number of errors in the received data.

2.2.2.1 MEDIUM ACCESS CONTROL

Medium access control (MAC) is achieved using a number of different techniques:

- Common channel, competition based method
- Time Division Multiple Access (TDMA)
- Frequency Division Multiple Access (FDMA)
- Code Division Multiple Access (CDMA)

2.2.2.1.1 COMMON CHANNEL, COMPETITION BASED METHOD

With this method, all nodes communicate on a common channel and compete for access to the medium. Carrier Sense, Multiple Access with Collision Avoidance (CSMA/CA) is discussed in greater detail in section 2.3.1, as it is used with the 802.11 WLAN standard. It will be explained in section 2.3.1 that this protocol causes significant degradation in performance when Internet data is transmitted across the network.

Akyildiz [2] stated that CSMA/CA techniques are inappropriate for sensor networks because they assume that traffic is distributed randomly. In reality, traffic may be periodic and is more congested in some areas of the network than others. Akyildiz suggested that an adaptive transmission rate control (ARC) scheme be employed that controls the amount of data originating from nodes so that other traffic may be routed efficiently through the network without being delayed by new traffic being generated by each node. The main advantage of CSMA/CA is that it requires minimal software and hardware resources at each node and does not require control messages to be passed between nodes.

2.2.2.1.2 TIME DIVISION MULTIPLE ACCESS (TDMA)

Nodes that use TDMA agree on a time slot when they may communicate. This method reduces the number of collisions with other transmitter nodes, but has the disadvantage of requiring additional overhead for time synchronisation. TDMA may be controlled by a central node or in a distributed fashion. The former process is used by Bluetooth (section 2.3.2) where nodes form small networks called Piconets and each slave node is given a time slot for communication with the master node. The problem with a centrally controlled scheme is that all nodes must be within range of the master node. Some technologies such as Bluetooth allow for communications

between Piconets. However, it will be explained in section 2.3.2 that the formation of inter-Piconet communication links has drawbacks.

A distributed TDMA protocol has been introduced and is called the Self-Organising Medium Access Control For Sensor Networks (SMACS) [2]. SMACS is activated when a node detects a neighbour. The two nodes then establish a transmission/reception schedule for communication.

2.2.2.1.3 Frequency Division Multiple Access (FDMA)

FDMA allocates each node pair a frequency of operation. This technique may be used in conjunction with the frequency hopping spread spectrum technique (appendix E.7.1). With frequency hopping, a node is given a frequency hopping code which dictates the order in which frequencies will be utilised. If two separate pairs of nodes have two different hopping codes, they will always use different frequencies of operation. A disadvantage of FDMA is that the hardware complexity is increased to allow the frequency of operation to be changed. FDMA also requires time synchronisation between each pair of nodes so that they change frequency at the same time.

2.2.2.1.4 Hybrid Approach

Shih [3] suggested that a hybrid TDMA/FDMA approach may be suitable for wireless sensor networks [2] where nodes operate in TDMA mode and vary the number of FDMA channels. In TDMA mode frequent transmissions take longer, because of the bandwidth restriction. Shih presented a formula to determine the optimum number of channels to minimise power consumption.

2.2.2.1.5 Code Division Multiple Access (CDMA)

CDMA is reviewed in appendix E.7.3 where it is shown that a device is able to demodulate data if it has the same code as the transmitter. All other signals that have been modulated with different codes are ignored by the destination. CDMA may be used as MAC protocol by allocating a code to each pair of devices. This allows devices to transmit at any time without interfering with any other nodes.

2.2.2.2 Error Control

The number of transmission errors may be reduced by increasing the transmitter power or using an error correction technique. In a wireless sensor environment, it is

required to minimise the power consumption. Therefore, it is preferable to use error correction techniques instead of increasing the transmitter power.

Error correction is a process where additional error correction data is transmitted with the useful data. The receiver uses the error correction data to calculate which bits of the useful data are corrupted so that they may be corrected. Error correction is a well documented area of research and a technique should be chosen that does not require excessive error correction data to be transmitted and requires minimal resources to compute.

2.2.3 NETWORK LAYER

The network layer is responsible for routing data from the source to the destination through the network. In a wireless sensor network, data is usually generated by the sensor nodes and forwarded to a 'sink' node. This network has a tree structure where each node sends data to a parent node which is one hop closer to the sink. Protocols that are designed for a tree topology do not require much overhead because nodes only need to monitor the surrounding nodes to determine the parent. A disadvantage is that it does not allow data to be sent in the reverse direction (from the sink to the sensor nodes) or between non-neighbouring nodes. Mesh networking is the alternative, which allows data to be sent between all nodes.

Routing protocols have received a great deal of attention from researchers and as such, many have been developed for WSNs. Since long range wireless sensor networks are sparse networks, the routing protocols are less important, since in these applications very few alternative network paths can exist. To provide sufficient background, a brief review is shown below.

A commonly cited publication is [4] by Broch who reviewed the performance of four common mesh routing protocols using a network simulator. The first protocol presented was the Destination-Sequence Distance Vector (DSDV) protocol which calculates the route to be taken as the packet reaches each node. Each DSDV node maintains a routing table which lists the "next hop" to get to a destination node. The nodes periodically transmit network maintenance messages to update the routing tables. This is a disadvantage of DSDV as it increases network traffic and reduces battery life.

The second protocol in [4] is the Temporally-Ordered Routing Algorithm (TORA). This protocol is designed to discover routes on demand, provide multiple routes to the destination, establish routes quickly and minimise communication overhead. TORA places the optimality of the route (shortest-path) as less important. The route is discovered by broadcasting a QUERY packet. Once this is received at the destination (or by a node that knows the route to the destination), it is sent pack to the transmitter via the same path so that the route may be determined. The disadvantage of TORA is that it transmits a large number of packets to determine a route.

A purely source routing protocol is DSR (Dynamic Source Routing). This protocol computes the route before the data is sent. The route information is placed in the data packet header and each node uses this information to find the next hop for the data. Source routing has the advantage that each node does not need to keep a routing table and there is no need for routing data to be transmitted across the network.

A combination of DSR and DSDV is utilised by the Ad Hoc On-Demand Distance Vector (AODV) protocol. It uses the on demand route discovery of DSR, but utilises the hop-by-hop routing of DSDV.

Broch tested these four protocols on the NS-2 network simulator. In the tests, Broch simulated the mobility of the nodes and assessed each protocol in terms of the number of successfully delivered packets, the amount of addition routing data and the utilisation of the shortest path. Broch showed that DSR had the best performance in all tests. TORA had significantly more routing overheads than the other protocols and DSDV delivered the least number of packets successfully.

Akyildiz [2] commented on routing algorithms and stated that power efficiency is also an important metric when finding a path. As such, some routing algorithms have been developed that compute the path of least energy (such as SMECN and SAR in Table 2-1). Table 2-1 provides an overview of the routing protocols discussed in [2].

TABLE 2-1: SENSOR NETWORK ROUTING SCHEMES [2]

Routing Scheme	Description
SMECN	Creates a subgraph of the sensor network that contains the minimum energy path
Flooding	Broadcasts data to all neighbour nodes regardless if they received it before or not
Gossiping	Sends data to one randomly selected neighbour
SPIN	Sends data to sensor nodes only if they are interested
SAR	Creates multiple trees where the root of each tree is one hop form the sink; selects a tree for data to be routed back to the sink according to the energy resources and additive quality of service metric
LEACH	Forms clusters to minimise energy dissipation
Directed Diffusion	Sets up gradients for data to flow from source to sink during interest dissemination

2.2.4 TRANSPORT LAYER

The role of the transport layer is to regulate the traffic flow between the source and the destination nodes. Little research has been conducted that attempts to propose a scheme or discuss the issues relating to the transport layer for a sensor network. It is stated in [2] that a transport layer protocol is particularly important if Internet data is to be routed over the sensor network.

A common transport layer algorithm that is used for Internet data is TCP (Transmission Control Protocol). TCP has a robust flow control mechanism that is well suited to the extreme conditions of the sensor network, however TCP uses large packet sizes that may be too big to be contained in the memory of each node. To overcome this, it may be necessary to split TCP packets into smaller sizes.

The focus on this project is on the lower layers of the protocol stack so the transport layer will not be investigated further.

2.2.5 APPLICATION LAYER

The application layer contains programs to be used by the end users. This is a largely unexplored area and only a small number of application layer protocols have been suggested. These include a sensor management protocol, task assignment and data advertisement protocol and sensor query and data dissemination protocol [2].

The design of the network stack allows lower layers to be altered with little affect on upper layers. This means that the application layer will not be affected by changes to the lower layers and therefore short-range application protocols may be used in the long-range system.

2.3 EXISTING WIRELESS TECHNOLOGY

A review of the existing wireless technology is necessary to determine which technologies, if any, are capable of operating as a long distance wireless sensor network (WSN). This review also aids in the system development since the advantages and disadvantages of each technology will be examined.

There are many wireless technologies available. Most are aimed at short-range applications and those that are long-range communications are usually too complex to be implemented in a WSN or require monthly usage charges. This section discusses the major wireless technologies and aspects of them which relate to a long-range WSN.

2.3.1 IEEE 802.11

The IEEE 802.11 protocol is also known as Wireless Local Area Network (WLAN) or Wi-Fi and is commonly used for wireless networking between computers. The WLAN protocol defines the physical and data-link layers of the protocol stack [5]. WLAN is capable of operating as an ad-hoc network if an upper routing layer is implemented.

There are several different versions of the 802.11 protocol, which are summarised in [5]. 802.11n is a new version of 802.11 which uses MIMO (multiple-input, multiple-output) and a larger bandwidth to achieve higher data rates than the previous versions of 802.11. The 802.11n devices use multiple antennas at the transmitter and receiver, where each antenna at the transmitter communicates with a specific antenna at the receiver. This allows for high data throughput via spatial multiplexing and increased range by exploiting spatial diversity.

TABLE 2-2: 802.11 SPECIFICATIONS [5]

	802.11a	802.11b	802.11g	802.11n
Max. Data Rate	54 Mbps	11 Mbps	54 Mbps	600Mbps
Range (indoor)	30m	35m	35m	70m
Modulation	OFDM	DSSS or CCK	DSSS or CCK or OFDM	DSSS or CCK or OFDM
Frequency	5 GHz	2.4 GHz	2.4 GHz	2.4 GHz or 5 GHz

Table 2-2 shows that the versions of 802.11 use different spread-spectrum modulation techniques. 802.11a/g uses OFDM to achieve high data rates, whilst 802.11b uses CCK (complementary code keying) which is CDMA technique, where the data is encoded using eight-bit numbers from a set of 64. At weak signal levels, 802.11b switches to DSSS (direct sequence spread spectrum) with BPSK or QPSK modulation to achieve communications at a lower data rate. 802.11g is designed to be backwards compatible with 802.11b and therefore also supports CCK modulation.

IEEE 802.11 devices operate in the industrial, scientific and medical (ISM) bands of 2.4 GHz or 5 GHz and are therefore limited to a range of several hundred metres. Communications over larger distances have been achieved with directional antennas, but these cannot be used in a WSN because nodes must communicate with neighbouring nodes in all directions.

802.11 implements two MAC layer protocols. These are point co-ordination function (PCF) and distributed co-ordination function (DCF). The former is not useful to wireless sensor networks, because the network operation is controlled by a central node and requires all devices to be in direct range. The latter is always implemented with or without PCF and is useful for wireless sensor networks as it allows devices to form an ad-hoc network if a suitable protocol is implemented in an upper layer.

DCF implements a Carrier Sense Multiple Access with Collision Avoidance (CSMA/CA) scheme that is also commonly used in wireless sensor networks. To transmit, a node must monitor the medium to ensure that no other nodes are transmitting. If a transmission is detected, the node must wait for a random time known as the ‘back-off period’. Once a message has been received, the receiving node notifies the sender using an acknowledgement packet (ACK).

Additionally, 802.11 specifies that transmitters must estimate the time required to transmit a data packet and append this to the message. The surrounding nodes use this time so that they know how long they must wait before the medium becomes available for usage. This allows the surrounding nodes to switch off their receivers to conserve power.

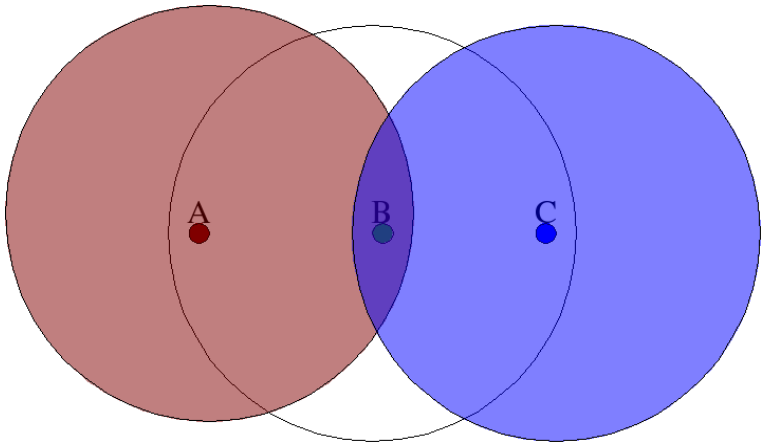

Figure 2-3: Hidden Node Problem

One problem with CSMA/CA schemes is the hidden-node problem that is described by Geier [6]. This is demonstrated by Figure 2-3, which shows three nodes and their transmission areas. Nodes A and C do not receive transmissions from each other, so it is possible that they may both transmit at the same time. The two transmissions will collide around node B and corrupt each other.

To correct this problem 802.11 utilises a scheme known as RTS/CTS (Request to Send/Clear to Send). With this method, a source node must request to transmit and a destination node must reply with 'clear to transmit'. In Figure 2-3, if node A would like to transmit to node B, it would first transmit a RTS message. Node B would hear this and send a CTS message. Node C would also detect the CTS packet and therefore knows not to transmit until node B has acknowledged that the transfer has been completed (ACK). Geier [6] stated that it is possible to conserve power by allowing node C to sleep until node B has transmitted the ACK. However, it was shown by Xu [7] and Hsieh [8] that the CSMA/CA and RTS/CTS schemes significantly degrade performance when the system is operating in 'ad-hoc mode' and TCP (Internet) data is transmitted across the network.

2.3.2 BLUETOOTH

Bluetooth was developed as a global standard for connecting mobile devices such as laptops, PDAs and mobile phones to form a Personal Area Network (PAN). Bluetooth devices operate in the 2.4GHz to 2.5GHz Industrial-Scientific-Medical (ISM) band [9] and have a range of 10m (low power devices) or 100m (high power devices). Bluetooth uses a fast hopping CDMA (FH-CDMA) scheme which is robust

against the high levels of interference that occur in the ISM band. A maximum data-rate to 723.2 kbps is achievable.

Bluetooth is a connection-oriented technology which requires devices to establish a communication channel before they converse. All devices belong to a network called a Piconet which is controlled by a master device. A Piconet can have 255 devices with only 8 active at a time [10].

Bluetooth can form an extended network by joining Piconets together to form a Scatternet. However, the Scatternet takes a considerable length of time to be formed and the link must remain active continuously. Research has been performed that investigates forming links on demand, but it has been shown that additional overhead is incurred to initialise the network [9, 11].

2.3.3 IEEE 802.15.4

The IEEE 802.15.4 standard defines the physical and medium-access layers for wireless personal area networks. The standard is designed for low power, low data-rate devices with multi-year battery life.

IEEE 802.15.4 devices operate in frequency bands of 2.4 GHz (typical), 915 MHz or 868 MHz with data rates up to 250 kbps. A direct sequence spread spectrum (DSSS) technique is used with Orthogonal QPSK (appendix E.4). The output power of the transmitter is generally 0dBm (1mW) which gives a transmission range of 10-75 m. The standard specifies that a CSMA/CA medium access protocol is to be used.

The IEEE 802.15.4 transceiver ICs are simple, inexpensive and have minimal external circuitry. An example is the Chipcon CC2420 [12], which is used in the MICAz (section 2.4.1) wireless sensor node that is produced by Crossbow Technology Inc. [13]. The short range of IEEE 802.15.4 means that this technology cannot be used in this project.

2.3.4 ZIGBEE

ZigBee defines a set of high-level communication protocols that use small low-power IEEE 802.51.4 radios. The ZigBee protocols, defined by the ZigBee alliance [14] are

intended for use in small embedded applications requiring low data rates and low power consumption. The current focus of ZigBee is to define a simple mesh networking protocol that can be used for industrial control, embedded sensing, building automation, etc. Zigbee devices are designed so that the battery will last for one to two years.

The ZigBee standard defines three types of nodes: ZigBee Coordinator (ZC), ZigBee Router (ZR) and ZigBee End Device (ZED). The ZC is the most capable device and is the root of the network tree and often bridges two networks. The ZR devices forward packets from other sources and the ZED is the most basic device that can only communicate with its parent.

ZigBee is designed for operation with short-range, battery-powered nodes that are typically deployed in high densities [14].

These IEEE 802.15.4 protocol devices are aimed at a range of markets including industry, consumer electronics, PC peripherals and personal healthcare.

2.3.5 Other Wireless Technologies

In some cities of the USA, ad-hoc radio networks are used by Ricochet Networks, Inc. [15] providing wireless Internet access to homes and mobile users. The back-bone of this system is comprised of an ad-hoc network of transceiver units that are positioned on the street light poles and operate at 2.4 GHz with a range of 0.4 to 0.8 km.

2.3.6 Long-Range Wireless Technologies

There are several long-range wireless technologies, but most of these operate in licensed bands and require periodic payments for their usage. Additionally, most of these technologies are too complex to be implemented in a low-cost WSN. An example is third generation (3G) mobile telephone technology which uses high-cost complex base-station receivers with high sensitivity, as well as large transmitter powers to achieve communications over long distances.

Another example is WiMAX, which is defined by the IEEE 802.16 [16] protocol. This is designed as a wireless broadband internet technology which delivers data over distances up to 10 km with a maximum data rate of 10 Mbps. WiMAX operates at

licensed frequencies and uses large transmitter power to achieve long-range communication.

2.4 Existing Wireless Sensor Nodes

To date, a number of wireless sensor nodes have been designed and produced. This section describes the nodes that are commonly used. All of these nodes can be programmed with TinyOS which is an open-source light-weight operating-system that was designed specifically for wireless sensor nodes. TinyOS contains implementations of many protocols and applications. It also includes a simulator, user-interfaces and debugging tools. TinyOS was used for this project and is discussed in further detail in chapter 5.

2.4.1 Crossbow Motes

Crossbow Technology, Inc. [13] produce several different wireless sensor nodes called Motes. The initial Mote (called the Mica, no longer produced) was designed by the Wireless Embedded Systems group at the University of California, Berkeley [17]. Crossbow has since produced subsequent motes such as the Mica2, Mica2Dot, Micaz, TelosB and Imote2. All of the devices consist of a microprocessor, radio transceiver, non-volatile memory and an expansion connector to connect to a sensor board. The hardware schematics for the Mica, Mica2, Mica2Dot and TelosB are publicly available on the TinyOS website [18].

The Crossbow developers are also major contributors to the TinyOS community. Additionally, Crossbow has released free software called MoteView, which allows data from a sensor network to be graphed and logged into a database. MoteView was adapted for this project and it discussed in further detail in chapter 5.

2.4.1.1 Mica2

The Mica2 uses an 8-bit ATMEL Atmega128L [19] processor (at 7.4 MHz) and a Chipcon CC1000 [20] radio transceiver. The CC1000 has an operational frequency range of 300 MHz to 1 GHz and has a configurable power output between -20 dBm and +10 dBm. The CC1000 uses binary frequency shift keying (BFSK) modulation and is capable of a 76.8 kbps data rate. The device has a quoted receiver sensitivity of -104 dBm (at 433 MHz with 19.2 kbps data rate, 20 kHz frequency separation and

BER < 1×10^{-3}) and a range of 150 m at 868/916 MHz and 300 m at 315 or 433 MHz under ideal conditions.

Figure 2-4: Mica2 Mote [13]

The Mica2 also has an ATMEL AT45DB041 4Mbit flash memory on board which is used for storing logged data and program images. This node has a 51-pin expansion connector for connection to stackable sensor boards. This connector is also used as a link to external programming/interface boards. Mica2 nodes are powered by 2 AA batteries and are quoted by Crossbow to last several years (depending on the application). Crossbow also produces the Mica2 in an OEM postage-stamp form factor. At the time of writing, a single Mica2 processor/radio board could be purchased for approximately $250AUD from Davidson Measurement [21]. Figure 2-4 shows a Mica2 Mote.

2.4.1.2 MICA2DOT

The Mica2Dot contains most of the same features of the Mica2, but is significantly smaller. The Mica2Dot is round and 25mm in diameter. This device operates at the same frequencies as the Mica2. The Mica2Dot has an 18 pin expansion connector for the sensor boards. Figure 2-5 shows a Mica2Dot mote compared with a coin. At the time of writing, the Mica2Dot was available from Davidson Measurement for $220AUD [21].

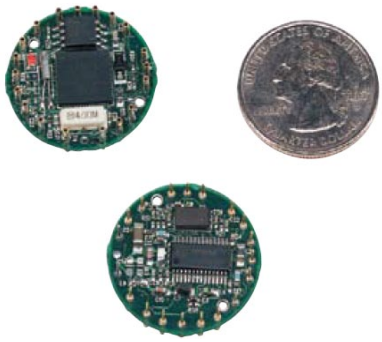

Figure 2-5: Mica2Dot Mote [13]

2.4.1.3 MICAZ

The Micaz is similar to the Mica2, but is IEEE 802.15.4 compliant (section 2.3.3). This device uses a Chipcon CC2420 transceiver IC [12]. Crossbow stated that the MICAz has an outdoor transmission range of 75 m to 100 m and indoor range of 20 m to 30 m. Crossbow also produce the Micaz as an OEM module which has a postage-stamp form factor.

2.4.1.4 TELOSB

The TelosB is another IEEE 802.15.4 compliant node that is produced by Crossbow. This device uses a 16-bit Texas Instrument MSP430 (at 8 MHz) microprocessor, which can be programmed directly using the on-board USB port. Some versions of the TelosB also have onboard temperature, humidity and light sensors. At the time of writing TelosB nodes can be purchased for approximately $260AUD (sensors included) [21]. Figure 2-6 shows a TelosB node.

Figure 2-6: TelosB Wireless Sensor Node [13]

2.4.1.5 IMOTE2

The Imote2 is new to the market and is described as the next generation of wireless sensor nodes, because it has very advanced processors. The Imote2 uses a 32-bit Intel Xscale processor (at 13 – 416 MHz) and has a wireless MMX DSP coprocessor. This

has substantially more processing power than the 7.4 MHz 8-bit processor used on the Mica2. Additionally, the Imote2 has 256 kB of SRAM, 32 MB of Flash and 32 MB of SDRAM. The Imote2 is aimed at applications which required complex digital processing such as image processing. For wireless communications the Imote2 uses an IEEE 802.15.4 compatible radio transceiver (CC2420). At the time of writing, the Imote2 could be purchased for $299USD (not including delivery to Australia).

Figure 2-7: Imote 2 Wireless Sensor Node [13]

2.4.1.6 OVERVIEW

The Mica motes are well established in the field and have been extensively tested in many applications. The schematics for the Mica motes are available for public use and alteration [22] and a large number of open-source software modules have been implemented in TinyOS, particularly for the Mica motes.

A major disadvantage for this project is that these nodes all have a short transmission range. The Mica2 mote was further investigated and used as the base for a long-range wireless sensor node which is discussed in chapter 4. By basing the design on this node, the development time of the node hardware architecture and software is reduced.

2.4.2 TMOTE SKY

The Tmote Sky (Figure 2-8) is a Zigbee compliant device that was originally designed by TinyOS developers [22] and is now produced by a company called Moteiv [23]. Tmote Sky is a 2.4GHz device that has a range of 125m. It utilises a Texas Instrument MSP430 processor that is TinyOS compatible. Tmote Sky uses an onboard antenna and transmits at powers ranging from –25dBm to 0dBm. This device is able to

transmit data rates of up to 250kbps. Optional on-board sensors are available to monitor the temperature, radiation or solar energy.

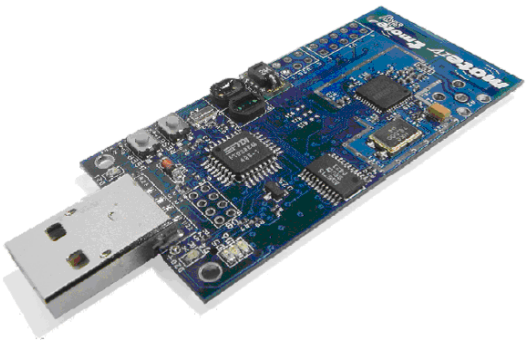

Figure 2-8: Tmote Sky Wireless Sensor Node [23]

For radio communications Tmote Sky utilises a Chipcon CC2420 transceiver module. This module is IEEE 802.15.4 compliant and provides the physical layer and some parts of the MAC layer. For transmission, the CC2420 utilises a direct-sequence spread spectrum technique with offset QPSK (OQPSK) modulation (appendix 2.2.1). Tmote Sky has six analogue inputs and four shared digital I/Os. Additionally, Tmote Sky has a USB connector so that it may be linked to a computer. A Tmote Sky node can be purchased for $130USD (not including delivery to Australia) [23]. Tmote Sky is a revision of the Telos node. The schematic for the Telos is available on the internet with the Mica Mote schematics [18].

2.4.3 EyesIFX Wireless Sensor Node

The EyesIFX wireless sensor node (Figure 2-9) [24] was developed as a result of research conducted on the Eyes project [25]. Eyes stands for **E**nerg**y** **E**fficient **S**ensor Networks and was a three year collaborative project on self-organisation and energy-efficient sensor networks. A consortium of European Universities and industry was involved with the project.

Figure 2-9: EyesIFX Wireless Sensor Node [24]

The EyesIFX wireless sensor node is now produced by Infineon Technologies AG [24] and is fully compatible with TinyOS. The EyesIFX node consists of a Texas Instruments MSP430 microprocessor (same as Tmote Sky), an Infineon TDA5250 radio transceiver, two environmental sensors, an expansion connector and a USB interface. The TDA5250 is a FSK/ASK transceiver IC which operates at 868 MHz with +4 dBm transmitted power. The transceiver is quoted to have a -109 dBm receiver sensitivity and handles data rates up to 64 kbps. The transmission range of the EyesIFX node is not quoted, but is expected to have short range since it transmits lower power than other nodes such as the Mica2. The Eyes project focussed on energy efficient sensor networks with nodes that output minimal transmitter power. The focus of the research was not on achieving long-range communications as is proposed with this project.

2.4.4 AMBIENT MICRO-NODE

The Ambient µNode (Figure 2-10) is produced by Ambient Systems [26], which was started by a group of researchers from the Eyes project [25]. The µNode uses a Texas Instruments MSP430 microprocessor and an 868/915 MHz transceiver with a data rate of 50 kbps. The transmitter has a configurable power output up to +10 dBm and the devices have a quoted outdoor range of 200 m. The µNodes can be installed with TinyOS or Ambient's proprietary operating system, AmbientRT. AmbientRT is a real-time Operating System which has features such as real-time scheduling and online configuration. Software modules can be loaded and unloaded in real-time.

Figure 2-10: Ambient µNode [26]

Ambient also produce a smaller node called the SmartTag which can interface with an Ambient mesh network. The SmartTag has a small microprocessor and radio transceiver and performs basic commands such as sending periodic measurements. This device is primarily designed for tracking applications. Business rules that define the SmartTag's operation can be programmed over the air.

2.4.5 FLECK NODE

The Fleck (Figure 2-11) was developed by the CSIRO Information and Communications Technology Centre [27] in Brisbane, Australia. The Flecks are based on the Mica2 [13] mote, use the same Atmel ATmega128L microprocessor and are programmed with TinyOS. The radio transceiver is a Nordic 903, which uses GFSK modulation and operates at 433 MHz. The Fleck supports data rates up to 72 kbps and uses an external antenna. The Fleck is stated to have a 500 m range, which is the longest range out of all the wireless sensor nodes identified in the literature review.

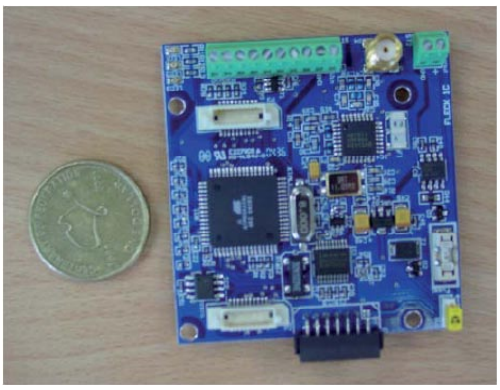

Figure 2-11: Fleck Node

2.5 EXISTING APPLICATIONS

2.5.1 BIRD HABITAT MONITORING

Kumagai [28] presented a bird habitat monitoring network based on an island called Great Duck Island off the coast of Maine, USA. A WSN consisting of Mica2Dot nodes was used to monitor the movement of a species of bird which lives in burrows around the island. Motes were placed in the burrows and trees and were used to measure the temperature inside the burrow and also detect the presence of the bird. The data from the network was sent to an on-site computer which forwarded results to researchers in California using a satellite link. This project demonstrated that a WSN can be used successfully for habitat monitoring. In this application, the transmission range of the nodes is short compared to the nodes presented in this project, but Kumagai used similar processors and software algorithms

2.5.2 VINEYARD SENSOR NETWORK

Mica motes have also been used to monitor the environmental conditions in a vineyard. Baard [29] described a system developed to monitor the temperature in a

five acre vineyard. Motes were positioned in the vineyard at distances of up to six metres apart. The data collected by the Motes allowed the temperature to be monitored across the entire area so that farming techniques could be altered to improve the quality of the product.

A similar project that utilised Motes to monitor a vineyard was described by Louis [29]. This project was undertaken in Margaret River, Western Australia where 22 Motes were deployed over 11 vineyards. The focus of the Western Australian project involved the data analysis techniques. In many systems, the quantity of data available is difficult to analyse. The Western Australian project authors plan to analyse and condense the data so that useful information is available to the end users.

Both of these projects are an example of how a WSN has been utilised to monitor environmental conditions to improve farming practices. These two examples also show the common usage of the Mica mote as a suitable and tested sensor node. The second example identified a problem that relates to difficulties involved with analysing the large quantities of data that are produced by a WSN.

2.5.3 LAWN MONITORING NETWORK

A lawn monitoring network called S.Sense is produced by a company called Digital Sun [30]. The system uses battery powered sensor nodes that are housed in spikes and pushed into the lawn at selected locations. Each sensor node monitors the soil moisture level and communicates with other nodes using an ad-hoc network. The measurements taken by the network are propagated to a control unit that activates relevant sprinklers when required. This system operates at 916MHz and each node has a transmission range of approximately 15 m.

Although the nodes have a small range, it shows how a sensor network can be utilised to control an environment in response to measurements and, in this case, improve the efficiency of water usage. The S. Sense system also demonstrated, on a smaller scale, the possibility of utilising the long-range network as a farmland irrigation control system.

2.5.4 Animal Movement Tracking Network

Wang [31] showed that a sensor network may be utilised to track the movement of a certain animal by monitoring its calling sound. Wang proposed that a sensor node could utilise digital signal processing (DSP) techniques to identify a particular animal by its calling sound. Wang used Pocket PCs as sensor nodes that were time synchronised. The time the animal call arrived at each node was compared and used to approximate the position using beamforming. Wang demonstrated the system using a frog call playing through a speaker and showed that the position was approximated within 250 mm in the worst case.

A similar system has been presented by Hu [32] to track the movement of cane toads in northern Australia. The system used Mica2 motes to take acoustic samples and forward these to microservers for further analysis. The microserver is a Crossbow Stargate which has a much more powerful processor (400MHz Intel PXA 255) than the Mica2 and implements a vocalisation recognition algorithm to determine the presence of cane toads. The Stargate nodes store the results in memory or can transfer the results to a user if connected to the internet or a satellite channel. A long-range wireless sensor network such as the one proposed in this project could also be used to relay the data to the user.

2.5.5 Industrial Process Automation

Wireless sensor networks are also being used for industrial process automation. The SmartWireless system by Emerson Process Management [33] is one such example. The system uses wireless sensor nodes to monitor temperature, fluid level or pressure. The sensor readings are forward to a gateway node which interfaces to an existing network. The SmartWireless system was developed by Dust Networks [1] (discussed below).

SmartWireless operates at 2.4 GHz with an IEEE 802.15.4 compatible transceiver or at 900 MHz with a proprietary transceiver. The system uses a time-synchronised mesh protocol (TSMP), which performs the tasks of the MAC and network layers [34]. This protocol uses a TDMA (section 2.2.2) MAC protocol that allocates a time slot for transmissions from each node. Additionally, the protocol uses frequency hopping (appendix E.7.1) which allows nodes to transmit at the same time without interfering

with each other. Since the nodes use IEEE 802.15.4 transceivers, there is additional noise immunity associated with the process gain of the DSSS (DS-CDMA) technique (appendix E.7.3) that is used by this protocol. Dust Networks claim that the FHSS/DSSS system has better noise immunity than Bluetooth and 100% reliability when subject to noise interference up to -60 dBm.

The network layer implements a redundant mesh protocol, where each node is associated with two parent nodes. Emerson stated that customer trials of the SmartWireless system have shown data reliability greater than 99%. This system is an example of a very robust, yet complex system which is aimed at densely deployed networks.

2.5.6 SMART DUST

The aim of many researchers in the field is to reduce the sensor nodes to a cubic millimetre in size. One team particularly interested in this area is the Intel research laboratories at Berkeley, CA, USA [35]. Intel envisages that these devices will be built completely on an integrated circuit and millions will be deployed world-wide.

Braunschweig [36] stated that the miniature sensor nodes could be utilised for a range of applications such as monitoring the power efficiency of a sky-scraper or monitoring chemical leaks in a fertiliser factory. Schmidt [37] stated that dust nodes may be scattered on a road in a battle environment to detect enemy movement.

Braunschweig has also presented a review of the current state of the ‘smart dust’ technology. At the time of being published, Braunschweig had identified four major commercial organisations that were developing a smart dust system, these are: Dust Networks [1], Crossbow Technology [13], Ember Corp. [38] and Millennial Net [39].

Dust Networks was founded by part of the team involved in the Mote development at UC, Berkeley [17]. Dust Networks aim at producing specific systems to be used for building automation, industrial monitoring and defence. Crossbow produce the Mote as described in section 2.4.1. Ember Corp. produce a number of radio transceiver ICs that implement the entire radio stack. A device called EM2420 is a 2.4GHz Zigbee compliant IC and is capable of transmission over 75m. A lower frequency device

called the EM1020 is also produced and has a range of 300m. Millennial Net produce a range of devices that implement a complete network. In this network, the end points are called I-Beans and are two cubic centimetres in size. These devices cannot communicate directly amongst themselves, but may communicate with a routing device that will pass messages across the network. The third device called a Gateway allows the network to be attached to a higher speed system such as 802.11. The endpoints have a range of 20 m, whilst the gateways and routers have a range of 30 m.

It should be noted that these companies are all aiming products at short-range communications. There seems to be minimal commercial interest in producing a wireless sensor network that is able to operate effectively over large distances.

2.6 CONCLUSION

It was shown in this literature review that current research is aimed at short-range, high-density networks. Major projects such as Smart Dust, shown in section 2.5.6 have focussed on the miniaturisation of nodes so that they may be deployed in high densities with minimal obtrusion. The majority of research relating to the network layers has also focussed on short-range communications. For example, Broch's simulation of routing protocols assumes that nodes move over a 1500mm × 300mm flat space [4]. In addition to this, Akyildiz [2] even defines a sensor network as being high in density with nodes having short-range transmission capabilities. This means that the majority of research relating to 'sensor networks', by this definition, assumes that nodes are high in density and hence have short transmission range.

Since most research has focussed on the development of short-range nodes, the feasibility of forming a wireless sensor network over a long distance is largely unexplored. Therefore, the investigation of a long-range wireless sensor network will have a significant contribution to knowledge.

3 Radio Propagation

The literature survey revealed that existing sensor nodes have a typical transmission range of several hundred metres and are usually deployed in a dense network with many redundant links. This redundancy means that the total network is very robust and reliability of a single link by itself is of little concern.

In contrast to this, the long-range wireless sensor network (LRWSN) has sparsely deployed nodes that are separated by large distances. The reliability of each radio link in this case is of concern since there are few redundant links in the network. To estimate the performance of each link it was necessary to develop a suitable radio propagation model. The development process of the model is discussed in this chapter, which commences by identifying the relevant radio propagation mechanisms, reviewing existing propagation models and then proposing an ideal model. A refined model is later recommended (section 3.6), which is based on the results of field-testing.

3.1 Propagation Mechanisms

The radio propagation mechanisms that were expected to affect the LRWSN were identified based on the radio specifications presented in Chapter 4. The specifications state that the LRWSN operates at a frequency of 40 MHz with 1 W EIRP and uses omni-directional antennas that are a quarter wavelength (1.8m) long. Radio links can be non line of site which means that the surrounding terrain has a large affect on the propagation of the radio signal. A summary of the identified propagation mechanisms is included below and was also published by Willis and Kikkert in [40]. This paper is contained in Appendix A.

3.1.1 FREE-SPACE LOSS

In an ideal environment, the power radiated by an antenna is spread uniformly over the surface of an imaginary sphere surrounding the antenna. Therefore, the power density at a point on the sphere decreases as the distance from the antenna increases. The free-space loss equation (1) gives the power received at a distance, d from the antenna [41].

$$P_r = \frac{P_t \lambda^2 G_t G_r}{16\pi^2 d^2} \tag{1}$$

where P_r and P_t are the received and transmitted power, respectively, G_t and G_r are the gain of the transmitter and receiver antennas, respectively and d is the distance from the transmitter.

In most real-world scenarios, the received power will be less due to the effects of reflected signals, obstructions and atmospheric conditions. In some cases, the signal strength is calculated using an approximated equation which adds a system loss factor L ($L \geq 1$) to the denominator of equation (1) to account for the additional losses.

3.1.2 REFLECTIONS

A reflection will occur when a transmitted signal is incident on a large specular surface. Reflections of the transmitted signal cause multiple signals to reach the receiver. This occurrence is known as multipath propagation, as demonstrated in Figure 3-1 which shows four signals that reach the receiver; these are the direct signal and three multipath signals that are caused by reflections off the surrounding objects. Each signal that reaches the receiver will have different amplitude and phase and may improve or degrade the overall signal.

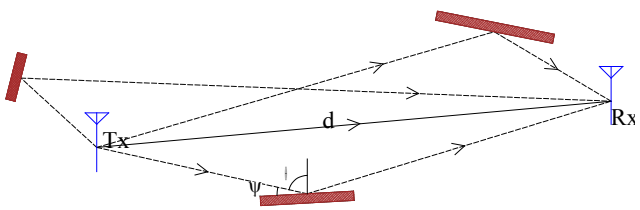

Figure 3-1: Multipath Propagation

At 40 MHz the wavelength is approximately 7.5 m. Therefore an object must be physically large in order to generate a reflection. It is envisaged that the LRWSN will be used in remote locations which are fairly barren. Therefore, it is not likely that there will be many reflected signals.

Parsons [42] showed that when a reflection is present, the received signal strength can be calculated using the reflection coefficient (Γ) as shown in equation (2).

$$P_R = \left(\frac{\lambda}{4\pi d} \left| 1 + \Gamma e^{j\Delta} \right| \right)^2 P_T G_T G_{R1} \qquad (2)$$

where $\Gamma = \dfrac{a \sin\psi - \sqrt{(\varepsilon_r - jx) - \cos^2\psi}}{a \sin\psi + \sqrt{(\varepsilon_r - jx) - \cos^2\psi}}$

$$x = \frac{\sigma}{2\pi f \varepsilon_0} = \frac{18 \times 10^9 \sigma}{f}$$

*w*here ψ is the angle of incidence (shown in Figure 3-1), ε_r is the relative dielectric constant of the ground, σ is the ground conductivity, ε_0 is the dielectric constant of vacuum and a = 1 or $(\varepsilon_r - jx)$ for horizontal or vertical polarisation, respectively.

Typical values of ground conductivity and dielectric constant are shown in Table 3-1. The magnitude of the reflection coefficient is given for the case of a 2 km link with 1.8 m high antennas operating at 40 MHz. It is obvious that the reflection coefficient for vertically polarised systems is more sensitive to changes in the conductivity or dielectic constant than a horizontally polarised system is. For vertical polarisation, the magnitude of the reflection coefficient is inversely related to the conductivity or dielectric constant. It should be noted that by increasing antenna height, the angle of incidence increases which causes the magnitude of the reflection coefficient to reduce.

TABLE 3-1: CONDUCTIVITY, DIELECTRIC CONSTANT AND REFLECTION COEFFICIENT

Ground	σ (S)	ε_r	| Γ (horz) |	| Γ (vert) |
Sea Water	5	81	1.0000	0.9404
Fresh Water	1×10^{-2}	81	0.9998	0.9838
Good Ground (wet)	2×10^{-2}	25 - 30	0.9997 ($\varepsilon_r = 25$)	0.9907 ($\varepsilon_r = 25$)
Average Ground	5×10^{-3}	15	0.9995	0.9928
Poor Ground (dry)	1×10^{-3}	4 - 7	0.9990 ($\varepsilon_r = 4$)	0.9958 ($\varepsilon_r = 4$)

In some applications, a wave can be reflected by the Earth's surface which can cause significant cancellation with the direct wave at the receiver and hence degrade the signal strength. The received signal strength can be calculated using the Plane-Earth Model (3), as shown by Hernando *et al.* in [41]. Hernando *et al.* explained that this equation is derived from the two-ray model (section 3.2.2) for long links with low antenna elevations.

$$P_r = P_t G_t G_r \left(\frac{h_t h_r}{d^2} \right)^2 \tag{3}$$

Hernando *et al.* [41] stated that this model applies to the situation in which low antennas are used and both ends have direct visibility of each other. It is envisaged that the nodes will be installed at ground level, thus meaning that the Plane Earth Model is not suitable for the LRWSN. A disadvantage of having low antennas is that the signal is attenuated by surrounding objects such as buildings and trees. This is less of a problem when using lower frequencies such as 40 MHz, as the obstacles are usually much smaller than the wavelength of the signal. This is particularly the case in a rural agricultural environment, where nodes are mostly surrounded by sparse vegetation.

3.1.3 Reflection Scattering

When a signal is reflected from a rough surface, the energy of the reflected ray will be dispersed and hence attenuated. This occurrence is known as scattering or specular reflection and was reviewed by Gibson [43] who stated that the roughness of a surface can be classified by the Rayleigh criterion .

$$h_c = \frac{\lambda}{8 \cos \theta_i} \tag{4}$$

where θ_i is the angle of incidence. Gibson [43] presented the parameter h which represents the minimum to maximum deviation about the mean terrain height. If $h > h_c$ then the terrain is considered rough and associated losses are accounted for by multiplying the reflection coefficient by a scattering loss factor ρ_s. This factor is calculated using Bothias' equation .

$$\rho_s = \exp\left[-8\left(\frac{\pi\sigma_h \cos\theta_i}{\lambda}\right)^2\right] \mathrm{I}_0\left[8\left(\frac{\pi\sigma_h \cos\theta_i}{\lambda}\right)^2\right] \quad (5)$$

where σ_h is the standard deviation of surface height about the mean surface height and I_0 is the 0^{th} order Bessel function of the first kind.

At the operating frequency of 40 MHz, the minimum value of h_c is 0.94 m for an angle of incidence of approximately 0^o. This value of h_c corresponds to extremely rough terrain that is unlikely to be experienced on typical rural agriculture land. As an indication, the value of σ_h is approximately 2.29 cm for bare ploughed land [44].

3.1.4 GROUND-WAVE PROPAGATION

When using ground-height vertically polarised antennas at low frequencies, the method of propagation is by ground-waves (Blake [45]). In this scenario, the radio wave aligns itself with the surface of the earth and can therefore travel beyond the horizon. The radio waves must be vertically polarised to minimise losses that would be caused by currents induced in the ground. However, there is a tendency for the wave to tilt toward the horizontal as the distance from the transmitter increases, hence causing losses.

Very long radio links can be established with ground-wave propagation. In some cases, using very low frequencies, these links can be around the world. Ground-wave propagation is very reliable and is almost independent of weather and solar conditions. Unfortunately, ground wave propagation usually occur at frequencies below 2MHz (Blake [45]) and will not affect the LRWSN. At higher frequencies, the signals are quickly attenuated due to increased loss in the currents induced in the ground.

3.1.5 EFFECT OF VEGETATION

A radio signal is attenuated when it travels through vegetation. The amount of attenuation is larger at higher frequencies. This was demonstrated by McLarnon [46] who summarised an ITU report [47] on the attenuation in vegetation. McLarnon stated that the attenuation caused by a forest is 0.4 dB/m at 3 GHz, 0.1 dB/m at 1 GHz and 0.05 dB/m at 200 MHz. Therefore, at 40 MHz the attenuation due to vegetation is predicted to be low. Additionally, the amount of vegetation would be small in most

farming applications. The lack of vegetation is demonstrated by Figure 3-2 which shows a typical Australian cattle farm. The radio propagation on this property is studied in section 3.5.3.

Figure 3-2: Aerial photograph of cattle farm

3.1.6 REFRACTION

A radio signal travelling across the Earth's surface follows a curved path that is caused by the variation in the refractive index of the atmosphere. A ray that travels into a medium with lower refractive index tends to bend away from the normal. The refractive index of the atmosphere decreases with height, which causes the radio wave to bend back towards the surface of the Earth and hence travel beyond the visible horizon. However, under standard atmospheric conditions the radius of curvature due to the atmosphere is greater than the radius of the earth and radio signals will tend to diverge from the earth's surface.

Hernando *et al*. [41] stated that normally in radio propagation studies, the Earth is assumed to have an effective radius of kR_0 where R_0 is the radius of the Earth (6370 km) and k is a correction factor that is usually assumed to be 4/3. This assumption accounts for refraction and allows radio paths to be modelled as straight lines. The k factor is dependent on atmospheric conditions, but is generally assumed to be 4/3.

The effective radio horizon for VHF and UHF systems can be approximated using equation (6) which is presented in the ARRL Antenna Book [48]. If an antenna is placed a quarter-wavelength (1.875 m) above the ground, the effective radio horizon is 5.65 km.

$$H_{eff} = 4.1224\sqrt{h} \tag{6}$$

where H_{eff} is the effective radio horizon in kilometres and h is the height of the antenna in metres.

If the receiving antenna is the same height as the transmitting antenna, then the link can be said to be line of sight if the nodes are less than $2H_{eff}$ apart and there are no terrain obstructions between the nodes. This corresponds to a distance of 11.3 km for two nodes raised a quarter-wavelength above ground. However, it should be noted that line of sight propagation will not occur because the Fresnel zone radius (see 3.2.6) at the mid-path is large.

3.1.7 Diffraction Loss

Diffraction occurs when the direct line between the transmitter and receiver is blocked by an obstacle that is much larger than the wavelength of the signal. The signal is scattered by the edges of the obstacle and is attenuated when the receiver is in the shadow of the obstacle. This is known as diffraction loss and is demonstrated in Figure 3-3 which shows a signal impinging on a knife-edge obstacle. Diffraction from a knife edge can cause a signal to bend behind the obstacle. It is also interesting to note that, as stated by Wong [49], the bending of the signal causes the signal strength to be considerably greater behind a knife-edge obstacle than it would be behind a rounded obstacle.

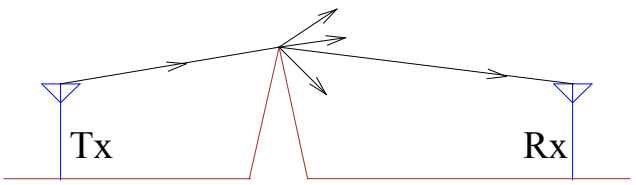

Figure 3-3: Diffraction loss caused by a signal impinging on a knife-edge obstacle

The diffraction loss caused by a knife-edge is easy to model, but knife-edges rarely occur in nature. It is important to model the effects of terrain features such as mountains and valleys. Additionally, the effects of diffraction due to propagation beyond the horizon must be modelled. Several theoretical and empirical models have been developed to estimate the diffraction loss over a given terrain. These models are reviewed in the next section.

3.2 Propagation Modelling

In order to develop an accurate radio propagation model for the LRWSN, it was necessary to review existing models to determine their suitability for the LRWSN application. Additionally, the weak and strong points of existing models were identified so that they may be applied in the design of the wireless sensor network propagation model (WSN model). The WSN model (section 3.3) uses a combination of the two-ray and PTP models described below.

This section commences with a discussion of multipath propagation and the two-ray model, followed by the more advanced radio propagation models that have been designed for systems operating in the UHF and upper VHF bands. These models are typically used to predict the strength of a television or mobile-phone signal in an urban environment.

3.2.1 Multipath Propagation

Signals that are reflected off large specular surfaces will arrive at the receiver with different magnitude and phase to the direct ray. The multipath components may improve or degrade the overall signal strength. The effect of the multipath components is illustrated by Figure 3-4 which shows a number of multipath signals ($\hat{M}_1$ - $\hat{M}_4$) acting on a direct signal ($\hat{D}$). The resultant ($\hat{R}$) has different magnitude and phase to $\hat{D}$.

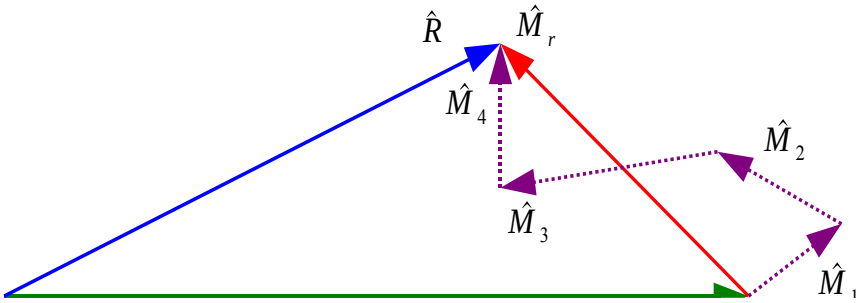

Figure 3-4: The effect of multipath signals

The strength of the multipath components can be calculated by summing the contribution of each ray. This method is applied in the Multipath Channel model in the AWR Visual System Simulator (VSS) [50] which uses equation (7) and (8) to find the signal strength for a sample *k*.

$$x[k] = \sum_{i=1}^{N} path(k,i) \tag{7}$$

where $x[k]$ is the *k*th sample, *N* is the number of multipath signal and $path(k,i)$ is the contribution of the *i*th multipath signal, determined by (8)

$$path(k,i) = A_i x(k - d_i) e^{j2\pi \frac{V}{C} f_c \cos\theta_i} \tag{8}$$

where A_i is the gain of *i*th path, $x(k - d_i)$ is the delayed sample associated with path *i* and $e^{j2\pi \frac{V}{C} f_c \cos\theta_i}$ represents the Doppler shift due to the movement of the receiver. However, in this case this effect can be ignored since the nodes in the LRWSN are fixed.

The multipath channel was implemented and built upon in the WSN model, which was developed in MATLAB. Identical simulations were conducted in VSS and MATLAB to test the MATLAB implementation. The simulations involved applying the Multipath model and additive white Gaussian noise (AWGN) to a binary phase shift keyed (BPSK) signal. Curves of BER versus SNR were produced by both models using identical parameters for the Multipath model. The VSS model is shown in Figure 3-5.

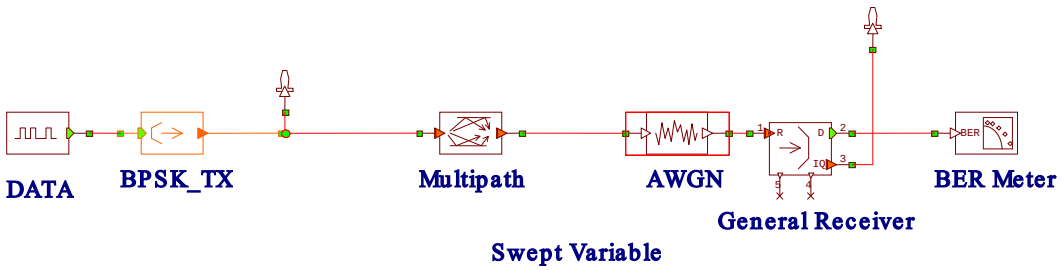

Figure 3-5: VSS model of a BPSK transceiver with multipath propagation

Figure 3-6 shows a comparison of the BER versus SNR curves derived from MATLAB and from VSS. These curves are similar and therefore verify the MATLAB model of the multipath channel.

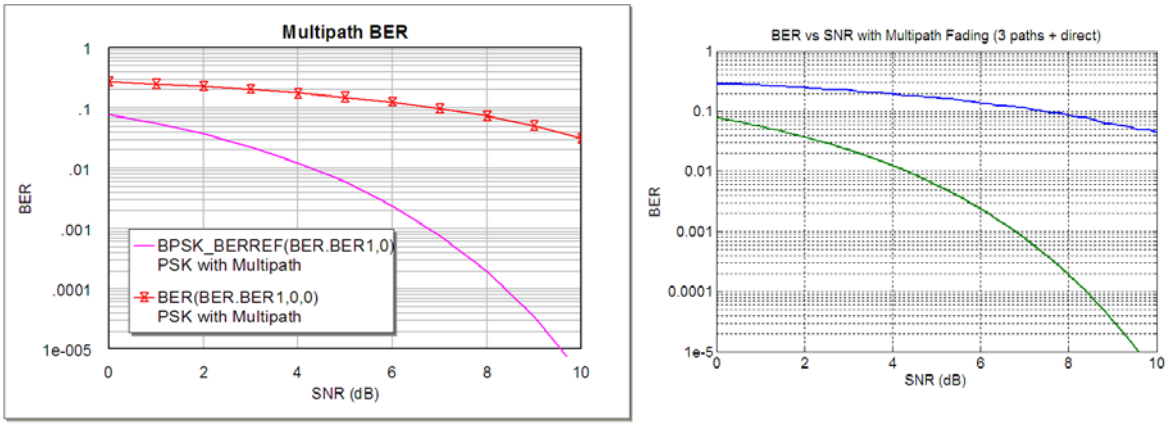

Figure 3-6: Comparison of BER vs. SNR for VSS (L) and MATLAB model (R)

3.2.2 Two-Ray Model

Neskovic *et al.* [51] presented the two-ray model which is a theoretical model commonly used for modelling a line-of-sight (LOS) radio channel. This model extends on the Multipath Model by calculating the magnitude of the reflection based on the reflection coefficient. The reflection coefficient (discussed in 3.1.2) is determined from the angle of incidence, ground conductivity, dielectric constant and antenna polarisation. The received signal strength is shown by equation (9) which sums the contribution of each path. This equation is derived from the free-space loss equation (1) and reflection equation (2), above.

$$P_r = P_t G_t G_r \left(\frac{\lambda}{4\pi}\right)^2 \left| \frac{1}{d_1}\exp(-jkd_1) + \Gamma(\psi)\frac{1}{d_2}\exp(-jkd_2) \right|^2 \qquad (9)$$

where d_1 and d_2 represent the length of the 1st and 2nd paths, respectively.

The Two-Ray Model is often used to describe the propagation of a direct ray and a ground-reflected ray. If this is the case, the value of ψ is very small for horizontally polarised long links and the reflection coefficient is approximately –1. This means that the direct and the ground-reflected waves will cancel. However, if the nodes are placed at ground level with bottom-fed quarter-wavelength antennas, the ground

reflection will not occur. This is because signals that are radiated downwards are injected directly into the Earth at the base of the transmitter. It was shown in section 3.1.2, that increasing the antenna height reduces the magnitude of the reflection coefficient. The effects of antenna height are further investigated in section 6.3.4.

The two-ray model can be extended to account for additional reflected rays. The components between the brackets in equation (9) represent the direct ray and the reflected ray, respectively. Additional rays of length d_n with reflection coefficient Γ_n can easily be added.

3.2.3 Multipath Signal Distribution

Hernando *et al.* [41] stated that instantaneous variations in the received signal envelope are usually characterised by a Rayleigh or Rician distribution. The Rayleigh distribution is used in cases where the direct component is not present and the received signal consists solely of multipath components. The probability density function for the Rayleigh distribution is shown in equation (10).

$$p(r) = \frac{r}{\sigma^2}\exp\left(-\frac{r^2}{2\sigma^2}\right) \quad \text{for } r \geq 0 \tag{10}$$

where $r(t)$ is the received signal envelope and σ is the standard deviation. Figure 3-7 shows the Rayleigh probability density function (PDF) and cumulative distribution function (CDF).

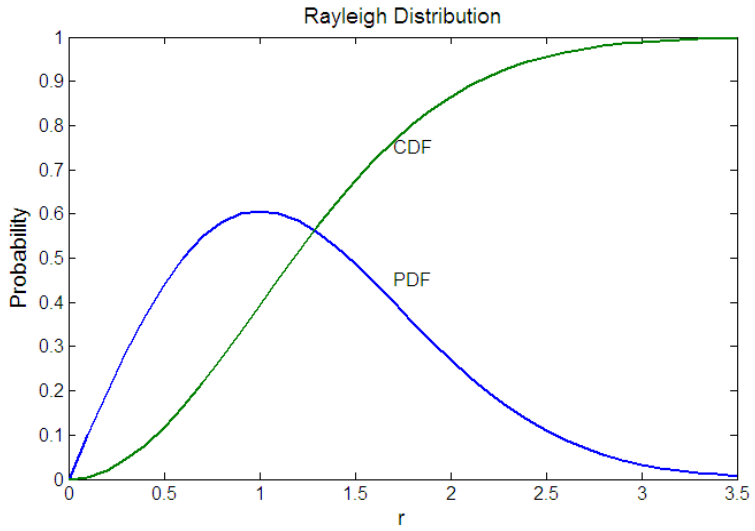

Figure 3-7: Rayleigh Distribution (standard deviation of 1)

When a direct component is also received with the multipath components, then the instantaneous variations in the received signal strength can be modelled as a Rician distribution (11).

$$p(r) = \frac{r}{\sigma^2} \exp\left[-\frac{r^2 + a^2}{2\sigma^2}\right] I_0\left(\frac{ra}{\sigma^2}\right) \qquad \text{for } r \geq 0 \tag{11}$$

where I_0 is the modified zeroth order Bessel function and the value of a depends on the strength of the direct component. When a is 0, the dominant signal is absent and the Rician distribution becomes a Rayleigh distribution. The Rician function is usually expressed in terms of the carrier-to-multipath ratio or k-factor (12).

$$k = \frac{c}{m} = \frac{a^2}{2\sigma^2} \tag{12}$$

where c and m are the strengths of the carrier and multipath components, respectively. Figure 3-8 shows $p(r)$ for various values of k (in dB). When k is 0 (the direct component is absent) $p(r)$ becomes a Rayleigh distribution. As the ratio of the direct to multipath components increases (K increases) the PDF shifts to the right indicating an increase in the strength of the received signal. For larger values of k, $p(r)$ becomes a Gaussian distribution.

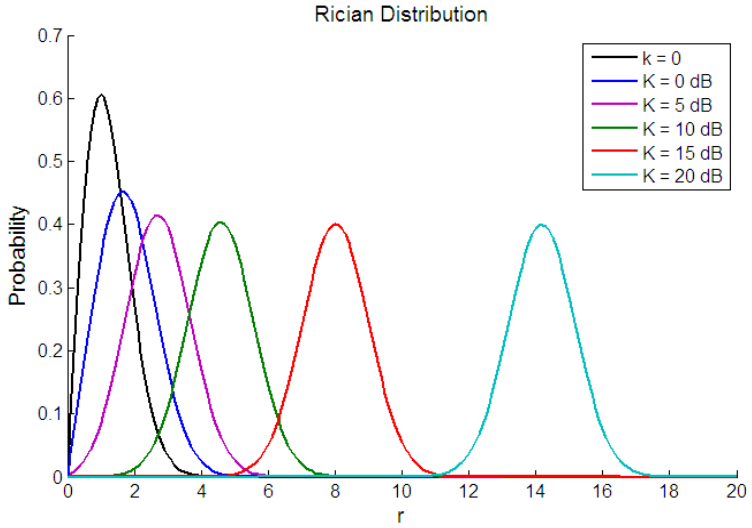

Figure 3-8: Rician probability density function for various values of k (standard deviation is 1)

3.2.4 OKUMURA-HATA MODEL

The Okumura model is a fully empirical model and a summary is provided by Hernando *et al.* in [41]. This model was developed from a set of measurements made in Japan at several frequencies used by common mobile communications services (up to 1920 MHz). The Okumura model uses a median field strength value which is calculated for a reference urban environment.

Correction factors are then applied to the reference value of median field strength to account for the environment type, terrain irregularity and antenna heights. These factors are determined from graphs that were derived from empirical data for frequencies in the range of 100 MHz to 2 GHz. The model has a large focus on radio propagation in an urban environment and is therefore not suitable for modelling the LRWSN as the nodes operate outside the frequency range of the model and are typically deployed in rural areas.

The Hata model is based on the Okumura model, but is designed to be used for computerised simulations of radio coverage [41]. Hata derived a set of formulae that are fitted to the values provided by the Okumura model. The Hata model is valid for frequencies in the range of 1500 MHz to 2000 MHz and is therefore not suitable for modelling the LRWSN.

3.2.5 THE IRREGULAR TERRAIN MODEL

The Irregular Terrain Model (ITM) is also known as the Longley-Rice model and was developed by Rice, Longley, Norton and Barsis, the authors of Technical Note 101 [52] which describes the model. The ITM is available as FORTRAN code [53] which has been summarised by Hufford in [54] who stated that the model can operate in two modes: area prediction mode and point-to-point mode. The former is commonly used to predict the signal strength of a broadcasting service over a specified area, whilst the latter is used to predict the signal strength between a transmitter and receiver. The point-to-point mode is most suitable for the LRWSN as it is required to analyse the radio link between two nodes.

Hufford [54] stated that the ITM model uses the following parameters in point-to-point mode:

- Distance between the nodes.
- Antenna heights.
- Carrier frequency.
- A terrain irregularity parameter.
- Mean surface refractivity.
- Effective curvature of the Earth.
- Radio climate which is expressed qualitatively as one of a number of discrete climate types.
- Surface transfer impedance of the ground, calculated from the permittivity and the conductivity of the ground.
- Distance from each node antenna to the radio horizon.
- Elevation angle of the horizons from each antenna.

The parameters relating to the terrain are derived from the terrain profile between the transmitter and receiver. The prediction of the model is dependent on whether the link is beyond the horizon or not. For line-of-sight paths, the model uses ray-optics theory. For paths with a common horizon, the Fresnel-Kirchoff knife-edge diffraction theory is applied and extended for rounded obstacles. For long distance paths, prediction is based on forward scatter theory, where rays are reflected by the troposphere. The ITM uses theoretical and empirical equations and Rice *et al.* [52] stated that the model has been tested for frequencies over the range of 40 MHz to 10 GHz.

The ITM can be set to output the reference attenuation which is the mean attenuation relative to the free-space loss. The model can also be configured to output a two-dimensional cumulative distribution of attenuation, which gives the probability that the attenuation will not exceed a given value for a given number of situations for at least a given value of time.

Wong [49] stated that the ITM computer program often makes anomalous predictions for distances less than 100 miles that are inconsistent with Technical Note 101 [52], the document on which it is based. Wong proposed an alternative model that tends to

resolve the anomalies. The alternative model is called the point-to-point (PTP) model and is discussed below. Figure 3-9 shows a comparison of the PTP model (blue) to the ITM (green), where it is illustrated that the PTP model gives predictions that are closer to the measured data.

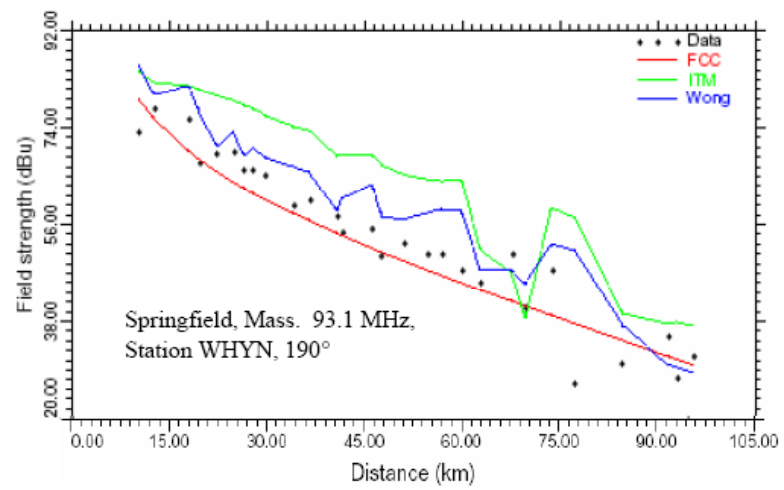

Figure 3-9: Comparison of the Irregular Terrain and the Point-to-Point Models [49]

3.2.6 PTP MODEL

The PTP model is based on the Longley-Rice model and is commonly used by the FCC for the prediction of FM and television signals. This model was described by Wong [49] who stated that the accuracy of the PTP model was as good as, or better than the Longley-Rice model. Wong also stated that the PTP model was particularly accurate at predicting the field strength due to terrain effects.

The PTP model calculates the signal loss due to the terrain by considering the following factors:

- The amount by which the direct ray clears or is blocked by prominent terrain obstacles.
- The position of the obstacle along the path
- The influence of the amount of roundness of the terrain
- The apparent curving of the ray due to refraction above the Earth's surface.

The effect of a terrain obstacle on the signal strength is calculated by determining the amount that the obstacle protrudes into the Fresnel zone that surrounds the direct ray.

Figure 3-10 shows an obstacle protruding into the Fresnel zone, which has a radius of A at this point. The distance between the obstacle and the direct ray is denoted as B. The B/A ratio is called the "path clearance ratio" and is used to determine the diffraction loss. A negative path clearance ratio indicates that the obstacle completely blocks the direct ray. Parameter A relates to the distance of the obstacle from the transmitter, therefore the path clearance ratio captures this information for the PTP model.

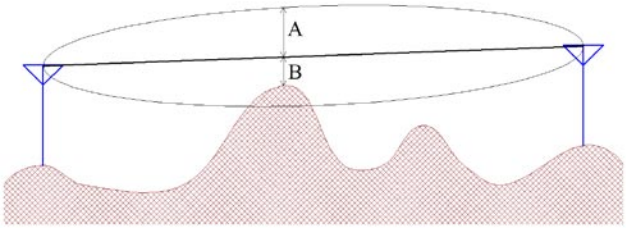

Figure 3-10: Measurements used to calculate the path clearance ratio

The diffraction loss caused by a knife-edge obstacle is less than that caused by a rounded obstacle. The PTP model incorporates this effect by calculating an "equivalent roundness factor". Wong [49] stated that terrain that is close to the obstacle has the largest affect on the path loss. Therefore, this terrain is analysed to determine the equivalent roundness factor. The equivalent roundness factor is determined by first comparing the variation of the terrain to a straight-line least-squares fit. This value is then scaled using a tested empirical formula to give the equivalent roundness factor. The equivalent roundness factor and path-clearance ratio are used to compute the path loss.

The PTP model incorporates the effect of refraction due to the Earth's surface by calculating a fictitious terrain height due to the effective Earth radius described above in section 3.1.6. The PTP model also incorporates the effects of secondary obstacles and propagation beyond the horizon.

3.3 The Wireless Sensor Network Propagation Model

The Wireless Sensor Network Propagation Model (WSN model) determines the BER based on the Signal-to-Noise Ratio (SNR), presented in section 3.3.1. The model predicts the effects of free-space loss, ground reflections, multipath reflections and

diffraction loss. The diffraction loss is predicted using the PTP model (section 3.2.6). A summary of the WSN model is provided in Table 3-2.

TABLE 3-2: SUMMARY OF WSN MODEL

Direct	Direct + ground reflection	Direct + ground reflection + multipath
Direct ray is estimated using: • Free-space loss (3.1.1) • Diffraction (PTP model - 3.2.6)	Summation of direct ray and ground reflection using eq (15) Ground reflection is estimated using: • Free-space loss (3.1.1) • Diffraction (same as direct 3.2.6) • Reflection loss calculated from angle of incidence and ground characteristics (3.1.2) • Phase shift (3.3.3)	Summation of direct ray, ground reflection and multipath rays using eq (15) Multipath rays are estimated using: • Free-space loss (3.1.1) • Reflection loss calculated from angle of incidence and ground characteristics (3.1.2) • Diffraction between reflector and Tx (3.2.6) • Diffraction from reflector and Rx (3.2.6) • Reflectors are imaginary and are positioned randomly on the terrain (3.3.3 / 3.3.4) • Phase shift (3.3.3)

3.3.1 BIT ERROR RATE AND SIGNAL-TO-NOISE RATIO

In order to determine the reliability of a radio link, it is necessary to determine the bit error rate (BER). The BER of a frequency shift keying (FSK) modulation scheme can be approximated using formula (13), which was presented by Haykin [55].

$$BER = \frac{1}{2}\operatorname{erfc}\left(\sqrt{\frac{E_b}{2N_0}}\right) \tag{13}$$

where erfc is the complimentary error function and E_b / N_0 represents the signal-to-noise ratio (SNR). Similar expressions are available for other modulation techniques.

Equation (13) shows that the BER can be calculated quite easily when given the SNR. Therefore, the aim of the Wireless Sensor Network Propagation Model (WSN model) is to determine the equivalent SNR for each link in the long-range ad-hoc radio system to be investigated.

The mean SNR is calculated by assuming that the signal component consists solely of the direct ray. The noise is assumed to consist of the thermal noise received by the antenna, the receiver noise factor and signal contributions from the multipath rays. Note that here, the multipath signals are considered to be noise since they cannot easily be used as part of the received signal. Instantaneous variations in the received

signal due to multipath fading are not predicted by the WSN model. However, it was shown above (3.2.3) that this can be approximated using a Rician distribution (direct signal plus multipath reflections) with a mean equal to the calculated SNR.

3.3.2 Strength of the Direct Component

The direct ray is subject to free-space loss (section 3.1.1) and diffraction determined by the PTP model (section 3.2.6). The diffraction is calculated using the terrain profile between the transmitter and receiver. This data can be extracted from digital elevation models provided by [56] or [57]. The received power is determined using equation (14).

$$P_{rd} = P_t L_{fs} L_d \tag{14}$$

where P_t is the transmitted power, L_{fs} is the free-space loss and L_d is the diffraction loss, as determined by the PTP model.

3.3.3 Strength of the Multipath Components

Each multipath ray is subject to loss due to the reflection, calculated using an extended form of the two-ray model equation (9) as shown below in equation (15).

$$P_{rm} = P_t G_t G_r \left(\frac{\lambda}{4\pi}\right)^2 \left| L_{d1}\Gamma_1(\psi_1)\frac{1}{d_1}\exp(-jkd_1) + \ldots + L_{dn}\Gamma_n(\psi_n)\frac{1}{d_n}\exp(-jkd_n) \right|^2 \tag{15}$$

where L_{dn} is the diffraction loss of the nth ray and $\Gamma_n(\psi_n)$ is the reflection loss of the nth ray which has an angle of incidence ψ_r. The phase of each ray is determined by the delay and is represented by the exp(-jkd_n) component, where d_n is the distance that the nth ray has travelled. This is equal to the sum of distances from the reflector to the transmitter and receiver.

The WSN model assumes that a reflector is an imaginary terrain feature or man-made object. The model assumes that this reflector can be positioned at any random point on the terrain. To calculate the reflection loss, a reflector is positioned at a random azimuth from the transceiver. The angle of incidence is chosen at random and the position of the reflector is calculated to allow the reflection to reach the receiver for

the given angle of incidence. The reflection coefficient is then computed using a random dielectric constant that is typical of the soil on an arid Australian farm. In the model a range of 2 to 7 is used, which is valid for dry soil and vegetation (2). At a small angle of incidence on dry soil, the variation in the dielectric constant has little affect on the variation of the reflection loss (a range of 2 to 7 causes a variation of 2% for a 1^{o} angle of incidence). In addition to the reflection loss, the scattering loss can be computed; however it was shown above in section 3.1.3 that this is negligible.

To compute the diffraction loss for the multipath signals, the terrain profile between the transmitter and receiver required for the PTP model is assumed uniform in the direction perpendicular to the direct signal path, as shown in Figure 3-11. Generally, rural Australia is very flat and this assumption gives a close approximation of the real terrain. However, if there is a large change in the terrain outside of the direct path, then this may affect the magnitude of the multipath components.

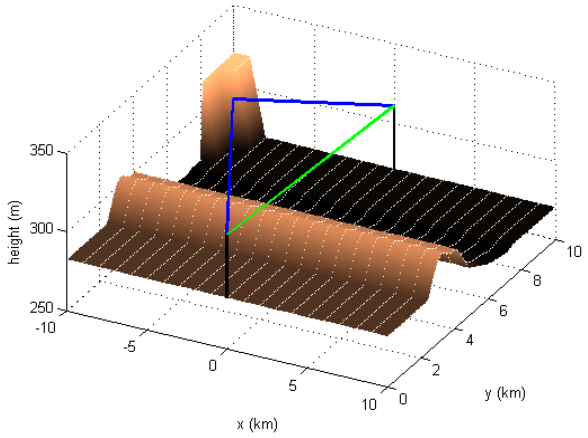

Figure 3-11: Terrain used for multipath signals, the terrain along x=0 is the actual path profile.

To model the diffraction loss, the multipath is treated as two paths (from transmitter to reflector and from reflector to receiver). The diffraction loss over each path is computed individually and then summed to give the total diffraction loss. The terrain profile for each path is approximated by taking a subsection of the terrain profile between the transmitter and receiver and elongating it so that it represents the distance between the reflector and transmitter or receiver. For example, in Figure 3-11, the terrain profile between transmitter (y=0) and the reflector is approximated by taking a subsection of the terrain profile between y=0 and y=8. This subsection is then

elongated so that it represents a distance of 11km (distance from transmitter to reflector). The terrain profile between reflector and receiver is similarly calculated by taking the terrain subsection between y=8 and y=10.

3.3.4 Positioning of the Reflectors

The WSN model uses a direct signal and a specified number of multipath signals, whose reflector positions and conditions are chosen at random. The model assumes that the reflection occurs at ground level. If the magnitude of a multipath signal is more than 30dB below the direct signal, then that path is discarded and a new path is generated.

This is demonstrated by Figure 3-12, which shows the cumulative random positions of the reflectors after 1000 simulations of propagation conditions with a direct path and two multipath reflections, which is typical of the expected environment. Such a simulation allows the expected long-term SNR distribution to be determined. It should be noted that the terrain modelled for this simulation is perfectly flat (z=0 for all positions).

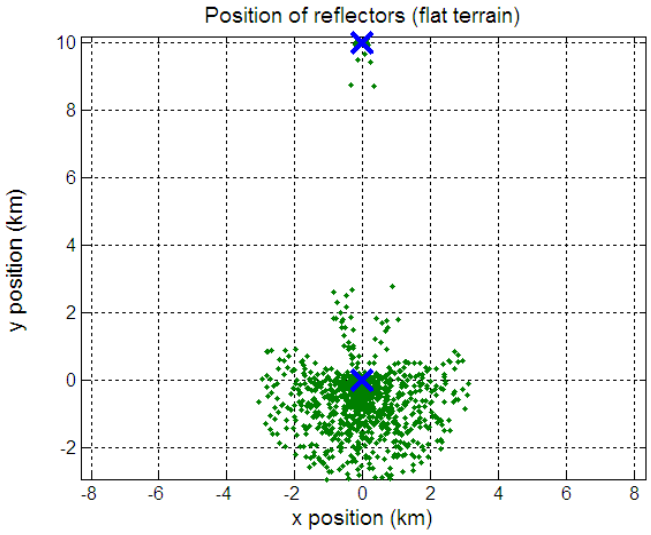

Figure 3-12: Cumulative position of reflectors after 1000 simulations (flat terrain).

In this figure, the transmitter and receiver are represented as crosses (the lower cross is the transmitter) and the reflectors are represented by dots. It is obvious in Figure 3-12 that the large majority of possible reflector positions are behind the transmitter. At these positions, the required angle of incidence will be large which incidentally causes a larger reflection coefficient and hence a stronger signal. It also evident that

there are some areas in front of the transmitter where there are no reflectors. At these points, the angle of incidence (approximately 20 degrees) causes the reflection coefficient to be very small and the multipath signal to be more than 30 dB below the direct signal.

The reflectors are fairly close to the transmitter because the diffraction loss from the PTP model increases sharply at approximately 3km so that reflections which include two paths greater than 3 km will result in negligible signals. Figure 3-13 shows the calculated diffraction loss at a given distance from the transmitter on flat terrain. It is evident from this figure that the diffraction loss increases dramatically approximately 3 km from the transmitter.

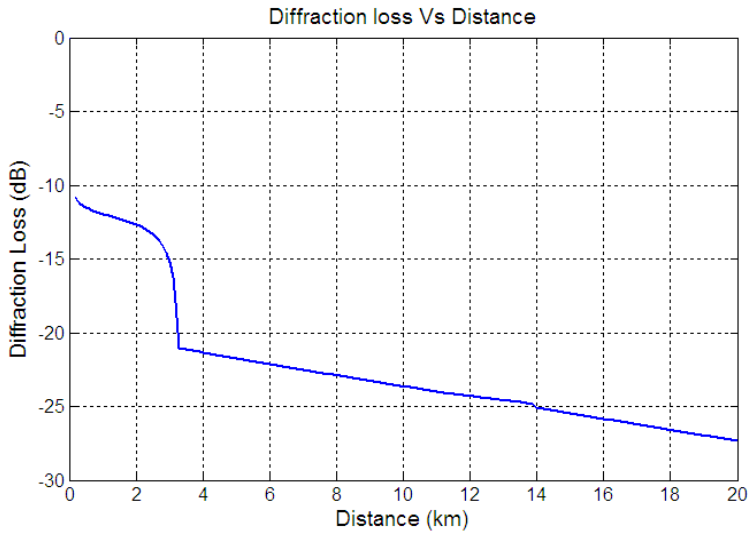

Figure 3-13: Diffraction loss computed by the PTP model for flat terrain

3.3.5 Verification of the PTP Model

The WSN model is heavily dependent on the PTP model, therefore it is important to verify that the PTP model is operating as stated by the author [49]. The source code for the PTP model is provided to the public [58] and is written in FORTRAN. This code was rewritten in MATLAB for use with the WSN model.

To ensure that the MATLAB version of the PTP gave the same results as the FORTRAN model, it was decided to compute the diffraction loss over the same terrain profile. Data collected by the Television Allocation Study Organization (TASO) for a number of test sites is given on the website for the PTP model [58]. A

comparison of this data with the PTP model is also included and one such comparison for the Fresno site is shown in Figure 3-14. Digital elevation data for this test site was sourced from the US Geological Survey [59] and input into the MATLAB version of the PTP model to give the predictions shown in Figure 3-15. By comparing Figure 3-14 to Figure 3-15, it is evident that the MATLAB version gives results that closely match the FORTRAN version. The small differences between these two figures are likely to be caused from differences in the terrain data used for the FORTRAN and MATLAB implementations of the model. For the site shown in Figure 3-14, the largest variations in predicted field strength occur at distances less than 50 km where the terrain is highly irregular and there is likely to be inconsistencies between the two terrain profiles.

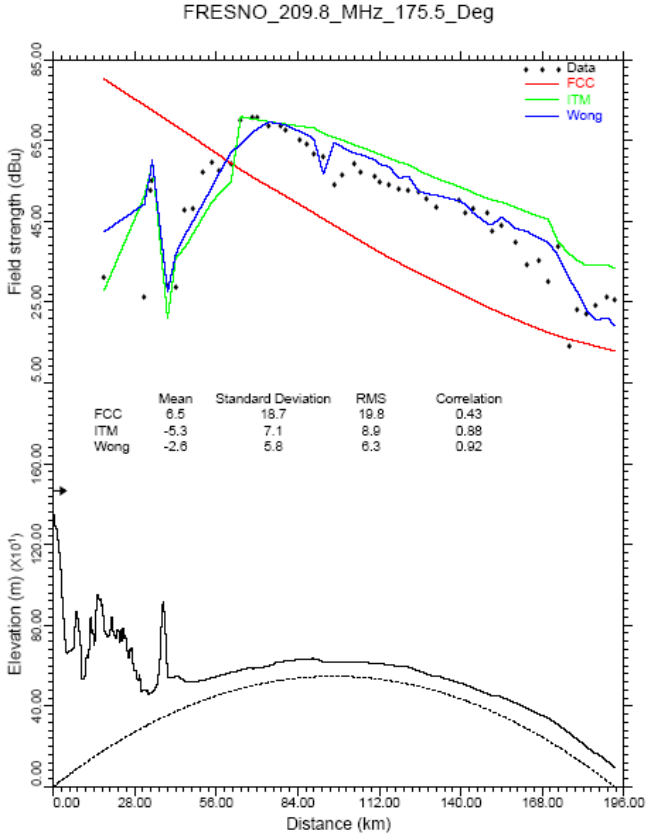

Figure 3-14: Collected data and PTP model prediction for a test site

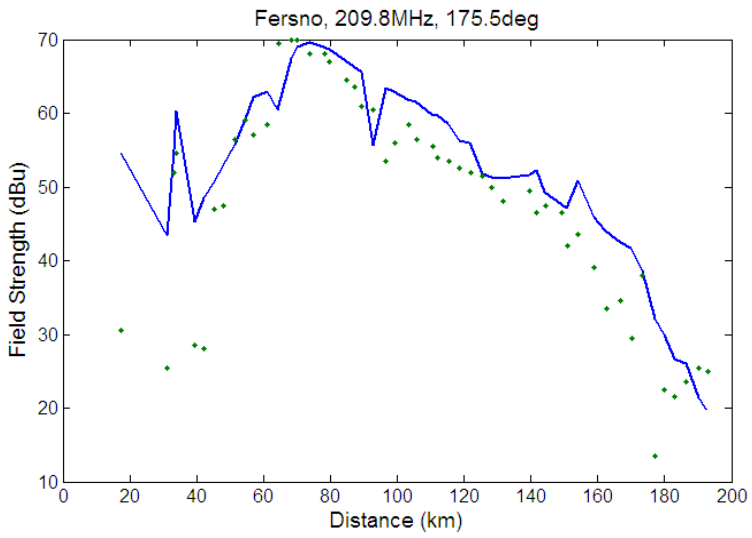

Figure 3-15: Comparison of PTP model (MATLAB version) predictions and collected data

3.4 Propagation Model – Program Structure

The program code of the WSN model is contained in Appendix K and follows the structure shown in Figure 3-16 and has been designed so that the user can automatically analyse all links on a given site or just an individual link. The WSN model requires terrain profile data between each set of nodes to find the diffraction loss. Terrain data for Australia can be downloaded from [56] or [57].

To analyse an entire site, the user must run `AnalyseSite.m` and specify the site name and the names of the first and last nodes to analyse. This function then calls `AnalyseLink.m` to perform an analysis for each link on the site. `AnalyseLink.m` uses `ReadPTPData.m` to load the terrain profile and then calls `CalcSNRPTP.m` 1000 times so that reflectors are positioned at 1000 random locations on the terrain. `CalcSNRPTP.m` calculates the SNR by considering the strength of the direct ray (calculated by `MultiRayPTPModel.m`) as the signal component and the multipath reflections as noise. The noise factor of the receiver is also considered, as well as thermal noise.

`MultiRayPTPModel.m`, positions a reflector at a random position on the terrain and uses `StretchTerrain.m` to determine the terrain profile to and from the reflector. The terrain data is passed to `PTPModel.m` which calculates the diffraction loss to and from the reflector. A multipath signal is rejected if its strength is more than

30dB below the direct ray. In this case, a new reflector position is determined and the signal strength is calculated.

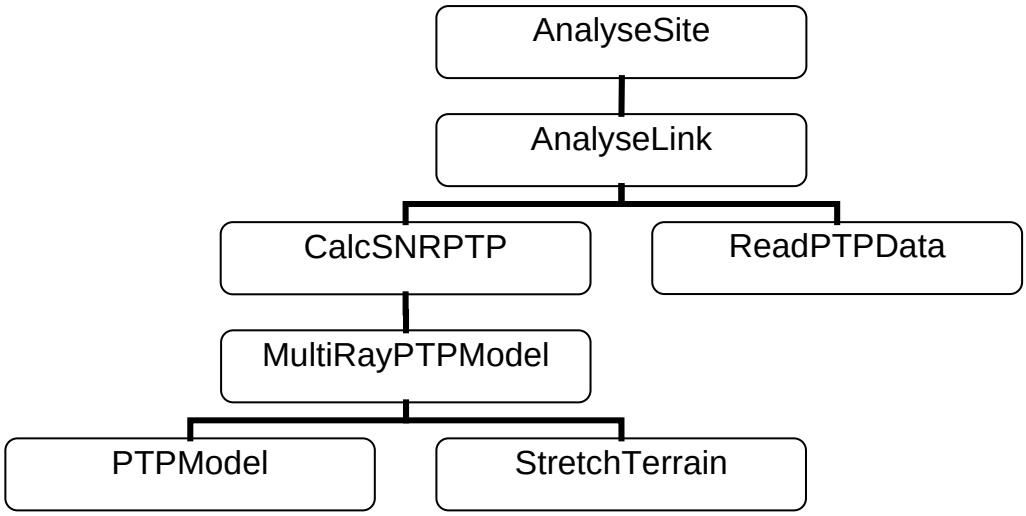

Figure 3-16: Structure of WSN model program code

3.5 Propagation Model Predictions

3.5.1 Effect of Multipath Signals

To examine the effect of the multipath signals, radio propagation was examined over ideal flat terrain (z=0 for all positions). Simulations were conducted at 40.8MHz with 1W EIRP. It was expected that the magnitude of the received signal could be represented as a Rician distribution since there is a direct ray reaching the receiver.

For reliable communications, a BER less than 10^{-3} is required, which corresponds to a SNR of 9.80dB, using equation (13). The WSN model predicts that a 10 km link over flat terrain will generate a 35.7 dB SNR when no multipath signals are present, thus easily meeting the 9.80 dB requirement. However, when multipath signals are included in the model, the SNR will decrease, as shown in Figure 3-17, which gives the cumulative SNR distribution obtained from 1000 simulations of the propagation model (reflection positions of simulation shown in Figure 3-12). Figure 3-17 shows the percentage of cases where the SNR is above a given level when a specified number of multipath signals are present. The graph shows that reliable communications can be established for more than 50% of the cases when there are 3 multipath signals or less. It is difficult to predict the number of multipath signals that

will occur in a real environment, but it is expected that this number will be small due to the large wavelength of the signal.

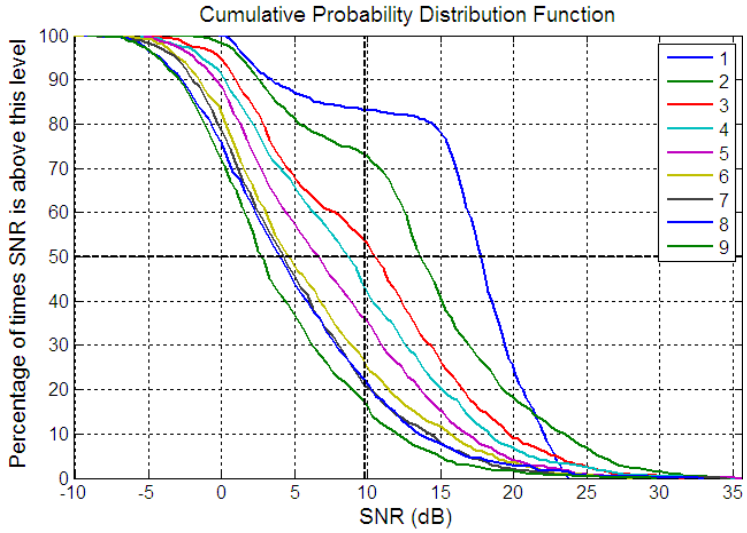

Figure 3-17: Cumulative probability distribution for the number of signals indicated in the legend.

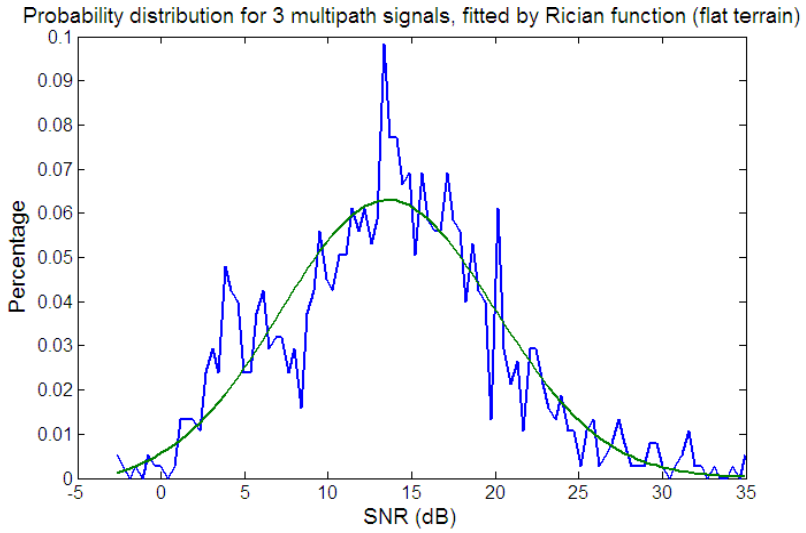

Figure 3-18: SNR probability distribution for 3 multipath signals, fitted by Rician function

Figure 3-18 shows the SNR probability distribution approximated by a Rician function, for the case where three multipath reflections are received with the direct signal. This figure shows that the best-fit Rician function is Gaussian in shape, which corresponds to a Rician function with a larger *k* factor (section 3.2.3). When six multipath components are received, the graph in Figure 3-19 was generated. In this case, the best-fit has a small *k* factor. This supports the theory presented in section 3.2.3 which stated that the *k* factor is equal to the ratio of the signal to the multipath components. A larger number of multipath components will cause a smaller *k* factor.

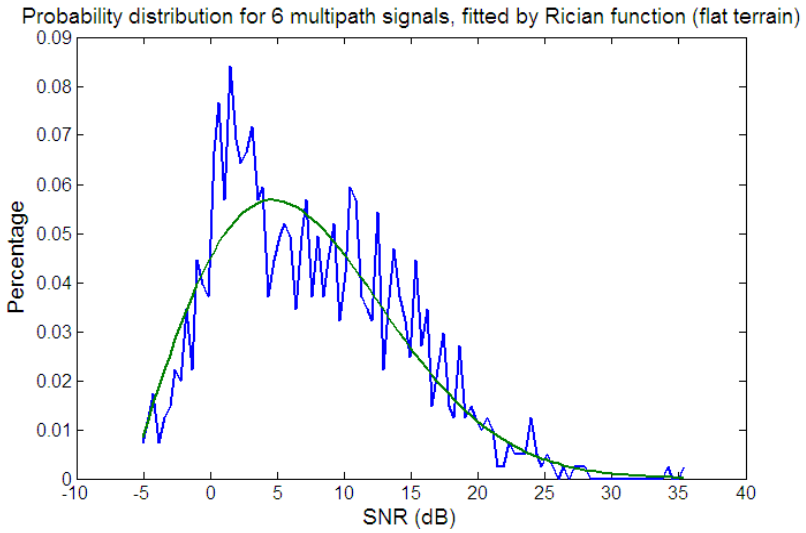

Figure 3-19: SNR probability distribution for 6 multipath signals, fitted by Rician function

3.5.2 The Effect of Irregular Terrain

To investigate the effect of irregular terrain, a case was studied where the transmitter and receiver are separated by a hill. For this investigation, it was assumed that the transmitter and receiver would be positioned on the terrain shown in Figure 3-20 (side profile of Figure 3-11), which shows a hill that is 25m higher than the transmitter and 35m higher than the receiver. Terrain that is not under the line-of-sight is assumed to have the same profile (see Figure 3-11). The model generates multipath signals by assuming there is some feature (not modelled) at the reflector position that is sufficiently large enough to generate a reflection.

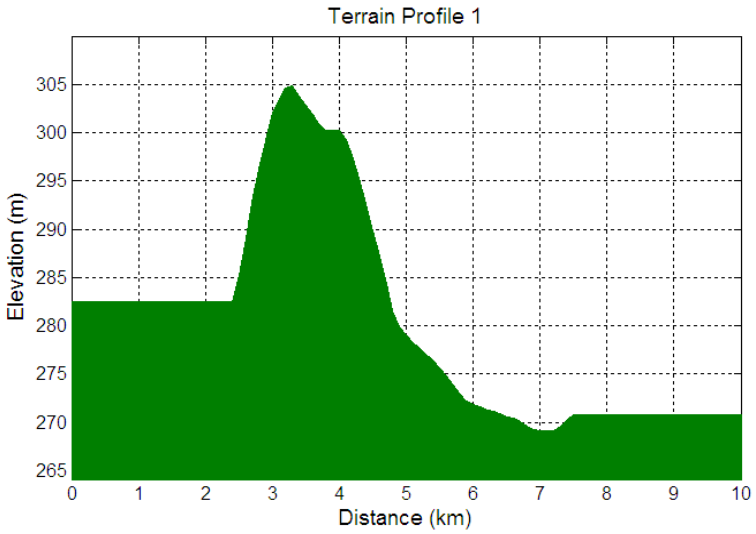

Figure 3-20: Terrain Profile 1

Table 3-3 shows a comparison of the minimum SNR occurring 50% of the time for flat and irregular terrain in the presence of a given number of multipath signals. This data shows that the SNR is generally less for propagation over irregular terrain; however, the differences are not exceptionally large.

TABLE 3-3: COMPARISON OF MINIMUM SNR OCCURRING 50% OF THE TIME FOR FLAT AND IRREGULAR TERRAIN

Number of multipath signals	SNR at 50% occurrence	
	Flat Terrain	Irregular Terrain
0	35.7	33.8
1	17.6	17.0
3	10.5	10.9
5	6.78	6.22

Figure 3-21 shows a comparison of the SNR probability distribution for links over flat and irregular terrain. It is evident that the distribution curve for irregular terrain has a similar shape to that of the flat terrain, but is shifted to the left. This indicates that the irregular terrain reduces the mean SNR.

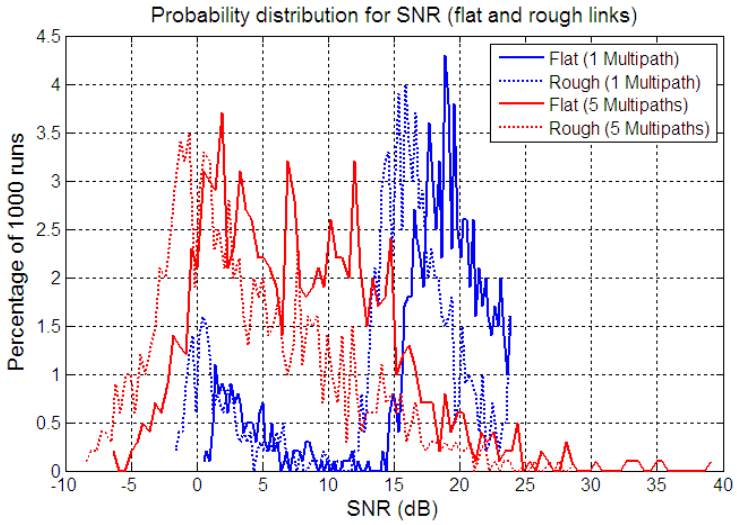

Figure 3-21: Comparison of distribution for flat and irregular terrain

3.5.3 CASE STUDY 1 – CATTLE STATION

As a case study, the WSN model was used to predict the SNR on a typical cattle station where a wireless sensor network could be used to monitor the level of water in cattle water troughs. Figure 3-22 shows a Google Earth satellite photograph of the cattle station, which is located 300 km west of Townsville, Australia. The property is

extremely isolated: 60 km from the nearest town, 10 km from the nearest bitumen road and 20 km from the nearest neighbour. In this figure, the nodes (A - F) are installed at the cattle troughs to measure the water level. The homestead is at node A and the furthest node (F) is over 10 km away. It would require most of a day to manually check the water troughs, hence the requirement for a wireless sensor network. The yellow lines represent links between sensor nodes and show the distance between nodes as well as the SNR exceeded 50% of the time. It is assumed that three multipath signals are present. The SNR is shown for signals propagating in the forward direction (e.g. C to D).

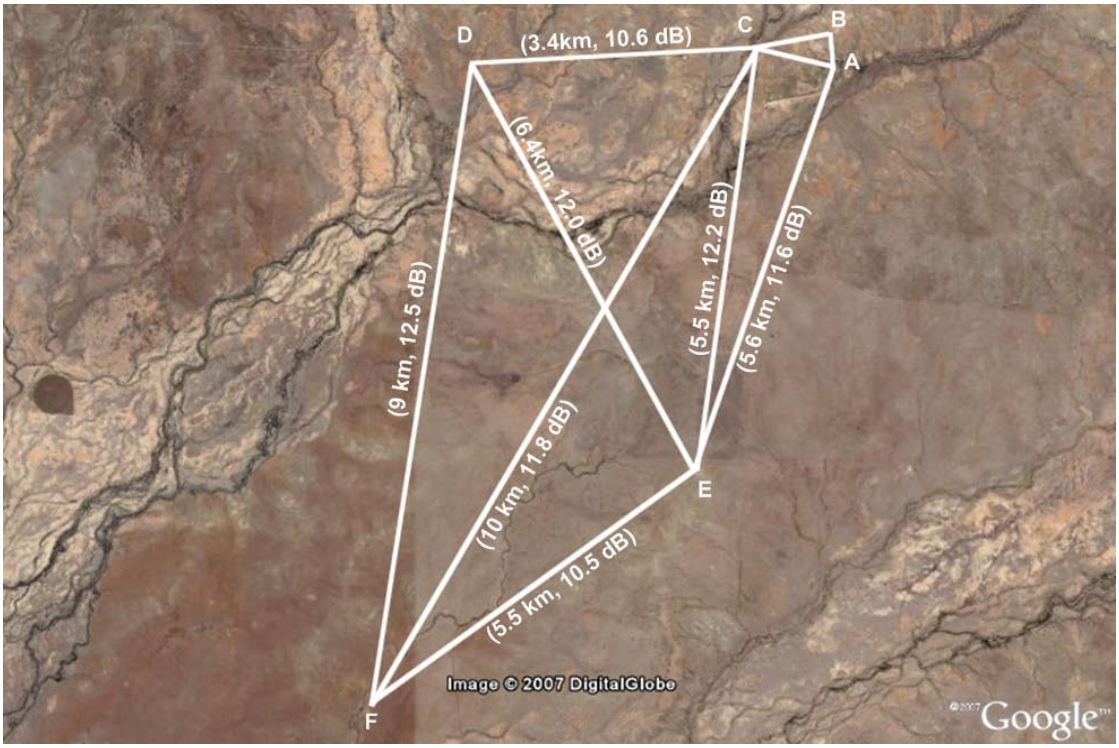

Figure 3-22: Map of Cattle Station for Case Study 1 [60] (Source: DigitalGlobe and Google)

It is evident that the SNR for all links in the case study is greater than 9.8dB which shows that the links between all nodes will be reliable. It should be noted that the terrain for this site is fairly flat, which explains why the SNR values are high. The smoothness of the terrain is demonstrated by the aerial photograph of the site, shown in Figure 3-2 (section 3.1.5).

3.5.4 Case Study 2 – Suburban/Rural Environment

As a second case study the site shown in Figure 3-23 was also analysed. This figure shows a satellite photograph of the regional city of Townsville, which contains nodes

(shown as crosses) in suburban and rural locations and has links (white lines) that travel over flat or mountainous terrain. The terrain in the centre of Figure 3-23 is very mountainous.

Some of the node positions shown in Figure 3-23 were later used in field testing presented in section 6.2. This site was chosen, because it has close proximity to James Cook University, which allowed for the hardware to be easily verified and adjusted. The site also incorporates suburban and rural environments, allowing the node to be tested in both scenarios.

Figure 3-23: Townsville test site. Used for case study 2 (Source: NASA World Wind)

Figure 3-24 shows a graphical representation of the sensor network for the Townsville site. In this figure, nodes are shown as stars and the SNR exceeded 50% of the time for each link is colour coded according to the legend shown. Radio links that are under the 9.8dB requirement are not shown. Some links were found to have a different SNR in each direction (shown as a combination of 2 colours). The SNR is different in each direction, because the PTP model calculates the diffraction loss to be different in each direction due to the position of the primary obstacle with respect to the transmitter. It will be difficult to obtain a reliable link to node PG as this link has a SNR of 11.39 dB in only one direction for the case of only one multipath signal.

Figure 3-25 shows the terrain profile from PG to JCU and gives a good indication of the mountainous nature of the terrain surrounding PG.

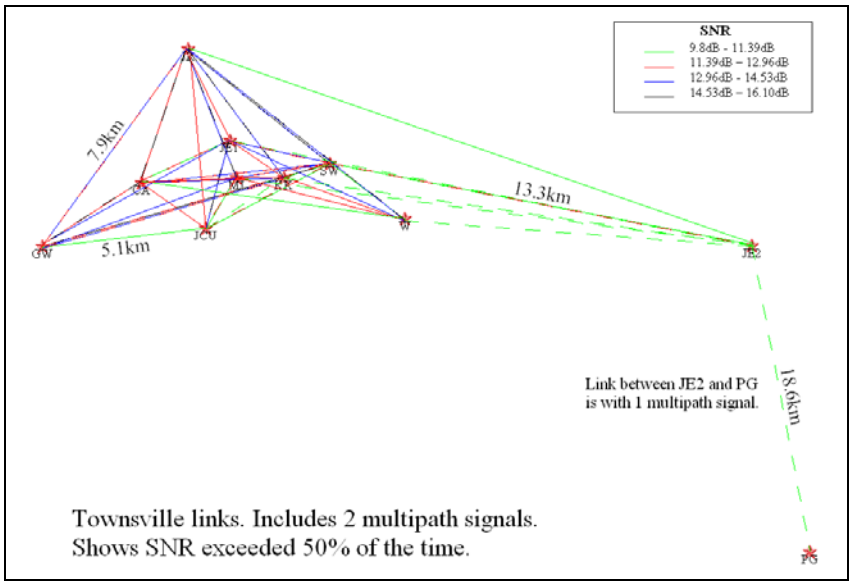

Figure 3-24: Graphical representation of the sensor network for case study 2

Figure 3-24 shows that some links will have a different SNR in each direction. This difference is due to the terrain profile between each set of links. For example, in Figure 3-25 the terrain is not symmetrical between PG and JCU. The primary obstacle is Mt Stuart and is located approximately 19 km from PG and 2 km from JCU. Therefore, the diffraction loss due to this obstacle, as computed by the PTP model will be different for the signals travelling in each direction.

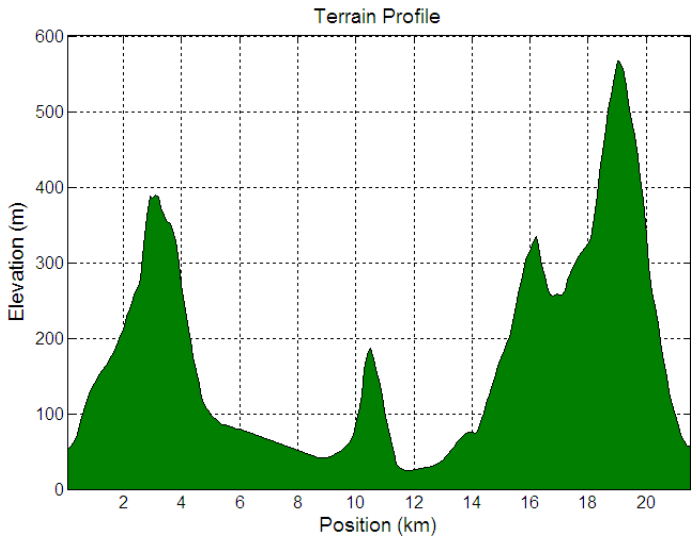

Figure 3-25: Terrain profile between PG (left) and JCU (right)

Figure 3-26 shows the possible reflector positions on the JCU to PG link, where JCU and PG are represented by the lower and upper crosses, respectively. This shows that the majority of possible reflectors would be positioned on the primary obstacle (Mt Stuart). Other reflectors are also shown on a second mountain located approximately 3km from PG.

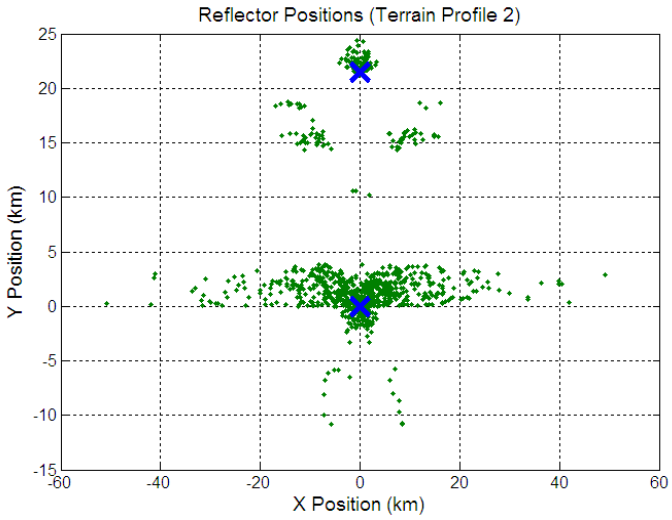

Figure 3-26: Possible reflector positions on the JCU to PG link

3.6 Refined Radio Propagation Model

Once the nodes had been designed and deployed the radio propagation model was refined to more accurately match the measured radio performance. This section discusses the refinements that were made to the model.

3.6.1 Antenna Elevation

When designing the antenna it was found that the nodes had to be raised above ground-level to allow for radials to be positioned around the base of the antenna at an declination angle of 30^{o} (Figure 4-28 of Section 4.8). The elevation of the nodes caused ground-reflections to occur that were not accounted for in the ideal propagation model.

The ground reflection is represented by its magnitude and phase (relative to the direct ray). The net received power is calculated by summing the contribution of the direct ray, ground reflection and multipath components using equation (15).

The phase difference between the direct ray and the ground reflection is determined from the path length of the ground reflected ray. The position of the reflection is determined by assuming that the terrain is flat and the transmitter or receiver (whichever is higher) is elevated by the difference in terrain heights. This is demonstrated in Figure 3-27, where the dashed green line represents the approximated terrain and the approximated reflection is shown as the dashed yellow line.

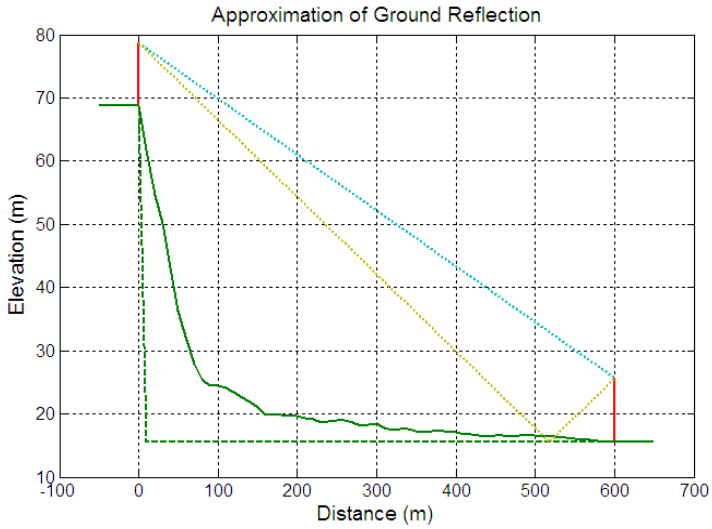

Figure 3-27: Approximated Terrain Profile for Calculation of Ground Reflection

The magnitude of the reflection is determined from the free-space loss, diffraction and the reflection coefficient. The latter is determined from the angle of incidence which is calculated using the geometry illustrated by Figure 3-27. For long links, the angle of incidence is very small and the reflection coefficient is close to 1. The diffraction loss is assumed to be the same as the direct ray since the ray path is very similar.

3.6.2 Receiver Noise Figure

The node receiver performance was analysed and the results are discussed in section 4.10.2. The noise figure was estimated using the SNR determined from the BER and the measured receiver sensitivity. A summary of the results is shown in Table 3-4. The receiver noise figure on each node was found to be larger than expected and the possible causes of this are discussed in section 4.10.2.

The measured noise figure is larger than the value used in the ideal propagation model. These measured values were used in the refined propagation model.

TABLE 3-4: CALCULATED NODE NOISE FIGURE

Node	Receiver Sensitivity (dBm)	Mean BER	SNR (dB)	Noise Figure (dB)
1	-70	2.93×10^{-3}	8.80	45.0
2	-81	1.45×10^{-3}	9.48	33.3
3	-79	1.66×10^{-3}	9.36	35.4
4	-78	2.49×10^{-3}	8.97	36.8

3.6.3 CALCULATION OF THE SIGNAL-TO-NOISE RATIO

The ideal propagation model calculated the SNR by assuming the signal solely consists of the direct ray and the noise component consists of the thermal noise, receiver noise figure and the multipath components. If the SNR is calculated using this method, then it cannot be confirmed with testing, because it is not possible to distinguish the direct component from the multipath components on the receiver.

The received signal strength is determined from the received signal strength indicator (RSSI) on the transceiver whilst a packet is being received. To allow the measured received power to be compared with simulations, the propagation model was altered so that it included the multipath components with the direct ray in order to calculate the net received power and the SNR. The measurements of received signal strength in several test environments are shown in section 6.

3.7 CHAPTER CONCLUSION

A long-range radio propagation model has been developed that is suitable for use with the LRWSN. This propagation model has shown that in the ideal case, reliable links can be achieved over distances of up to 10 km. The SNR has been calculated for links in two separate environments: a rural cattle farm and a suburban/rural environment (Townsville). Refinements to the ideal model have been presented that are based on hardware measured presented in Chapter 4 and the results of field testing presented in Chapter 6.